TU Delft

Delft University of Technology

Document Version
Final published version

Licence
CC BY

Citation (APA)
Tsioni, V., Kammouh, O., & Nogal, M. (2026). Recovery optimization of water distribution networks following seismic events. *Resilient Cities and Structures*, *5*(3), 158-181. https://doi.org/10.1016/j.rcns.2026.07.004

Important note
To cite this publication, please use the final published version (if applicable).
Please check the document version above.

Copyright
In case the licence states “Dutch Copyright Act (Article 25fa)”, this publication was made available Green Open Access via the TU Delft Institutional Repository pursuant to Dutch Copyright Act (Article 25fa, the Taverne amendment). This provision does not affect copyright ownership.
Unless copyright is transferred by contract or statute, it remains with the copyright holder.

Sharing and reuse
Other than for strictly personal use, it is not permitted to download, forward or distribute the text or part of it, without the consent of the author(s) and/or copyright holder(s), unless the work is under an open content license such as Creative Commons.

Takedown policy
Please contact us and provide details if you believe this document breaches copyrights.
We will remove access to the work immediately and investigate your claim.

This work is downloaded from Delft University of Technology.

Resilient Cities and Structures 5 (2026) 158–181

Contents lists available at ScienceDirect

Resilient Cities and Structures

journal homepage: www.elsevier.com/locate/rcns

Recovery optimization of water distribution networks following seismic events

V. Tsioni [a], O. Kammouh [b,*], M. Nogal [a]

[a] Faculty of Civil Engineering & Geosciences, Delft University of Technology, Netherlands
[b] Faculty of Technology, Policy, and Management, Delft University of Technology, Netherlands

ARTICLE INFO

Keywords:
Water distribution networks
Resilience
Optimization
Recovery sequence
Characteristic curves

ABSTRACT

Water Distribution Networks (WDNs) are critical infrastructure systems essential for maintaining urban functionality. Ensuring their continued operation, particularly in the aftermath of disasters, remains a significant challenge. Despite the growing attention to resilience, existing assessment methodologies do not sufficiently incorporate the post-disaster recovery process. This paper introduces an optimization-based framework aimed at enhancing the seismic resilience of WDNs by determining optimal pipeline repair sequences. The proposed approach employs a Genetic Algorithm to prioritize pipeline repairs, maximizing the efficiency of the recovery process. Based on the optimized repair sequence, characteristic resilience curves are developed, providing a comprehensive assessment of network performance under various seismic intensities and resource constraints. The model's scalability and applicability are validated through case studies on networks of differing scales. Results from this integrated methodology yield critical insights into network recovery dynamics, serving as valuable guidance for asset managers, engineers, and policymakers in planning, resource allocation, and decision-making for seismic risk mitigation and efficient infrastructure recovery.

1. Introduction

Water Distribution Networks (WDNs) are a fundamental element of critical infrastructure systems. They are considered essential to the resilience of urban environments – their failure or degradation may have serious consequences for public health, safety, economic stability, and environmental protection [1,2]. These systems also play a key role in supporting economic growth and preserving urban and natural ecosystems.

Due to their extensive spatial distribution and high degree of interconnectivity, WDNs are particularly susceptible to both natural and anthropogenic hazards. In many cases, critical components are located underground, which increases their vulnerability to seismic events. Earthquakes, in particular, can cause extensive damage to pipelines through soil-pipe interactions, resulting in widespread service interruptions that are often difficult to isolate and repair. In addition, the functionality of WDNs depends on other infrastructure systems, including transport and power grids [3]. Disruptions to these interconnected systems can propagate, exacerbating the impact on water services. The unpredictability of natural hazards, especially earthquakes, combined with the cascading effects of interdependent infrastructure failures, poses significant challenges for asset owners and decision-makers responsible for maintaining the operational continuity of WDNs.

Traditional approaches to risk management in WDNs have predominantly focused on the physical protection of assets in order to minimize the consequences of hazard events [4]. These methods treat the occurrence and the intensity of the hazard probabilistically [5], but the protection they inform is designed for a chosen hazard level, and damage still occurs when that level is exceeded. What they quantify is the expected damage and its direct cost, rather than the time the system needs to return to service. The engineering community has come to recognize that long repair and reconstruction periods cause a loss of functionality whose impact reaches beyond the initial damage [6], and this recognition has driven a gradual shift in recent decades towards resilience-based frameworks. Resilience, commonly defined as the capacity of a system to prepare for, absorb, adapt to, and recover from disruptive events [1], places emphasis not only on preventing damage but also on maintaining system functionality before, during, and after a disruptive event. Various methodologies have been proposed for assessing the resilience of WDNs [7,8], which can be broadly classified into two principal categories: surrogate measures and recovery-based simulations.

* Corresponding author.
E-mail address: o.kammouh@tudelft.nl (O. Kammouh).

https://doi.org/10.1016/j.rcns.2026.07.004
Received 12 January 2026; Received in revised form 22 July 2026; Accepted 31 July 2026
Available online 20 August 2026
2772-7416/© 2026 The Author(s). Published by Elsevier B.V. on behalf of College of Civil Engineering, Tongji University. This is an open access article under the CC BY license (http://creativecommons.org/licenses/by/4.0/).

The first category, known as the surrogate measure approach, uses indirect metrics to estimate resilience by analyzing network characteristics without explicitly modeling recovery dynamics. These surrogate metrics can be grouped into three main types: energy-based, entropy-based, and graph-theoretic. Among energy-based metrics, the most widely used is the Resilience Index introduced by [9], which evaluates the surplus hydraulic power relative to the minimum required to satisfy demand. While effective in looped networks, its relevance diminishes in sparse systems. To address this, extensions have been proposed to incorporate structural features, such as loop diameter uniformity [10] and pressure shortfalls [11]; the original formulation has also been generalized for use with pressure-driven modeling and leakage [12]. Entropy-based methods, such as those using Shannon entropy [13] and Tsallis entropy [14], quantify flow distribution and redundancy to reflect adaptability. Although computationally efficient, they often overlook structural and economic constraints. Graph-theoretic approaches model WDNs as mathematical graphs and evaluate topological robustness through metrics like connectivity, clustering coefficients, and betweenness centrality [15–17]. While providing useful insights into network structure, they typically neglect hydraulic behavior and dynamic system responses. Despite their differences, all three types of metrics share a common limitation: they are static approximations and do not capture the temporal or operational complexities involved in real recovery processes.

The second major category comprises simulation-based approaches, which explicitly model the temporal dynamics of post-disaster recovery [18]. These methods simulate how system performance evolves in response to interventions such as pipeline inspection, repair scheduling, and resource deployment. For instance, [19] used Discrete Event Simulation Models (DESMs) to demonstrate the impact of repair sequencing on recovery. However, DESMs require detailed input data and are often computationally intensive, limiting their scalability. To address this, [20] integrated resilience metrics into DESM frameworks to account for interdependencies, though at the cost of increased complexity. Several studies have also explored targeted strategies to enhance resilience, such as retrofitting pipelines [21], upgrading pumping systems [22], or developing multi-dimensional indices incorporating user demand, tank capacity, and water quality [23]. These interventions provide useful planning insights but often depend on granular data not widely available. A related stream of work involves optimization-based frameworks, which aim to identify effective repair strategies under resource and time constraints. Examples include models that coordinate interventions under limited budgets [24], integrate hydraulic simulations to assess repair sequences [25], or apply adaptive strategies that evolve with changing conditions [26]. These approaches offer a strong analytical value but are computationally demanding and less suited for real-time or large-scale application. Across simulation-based research, one recurring theme is the identification of damaged pipelines as the primary bottleneck to restoring service [2,25–27]. In response, [27] proposed a phased recovery framework with demand prioritization and staged service restoration. However, such models require high-resolution consumption and damage data, which may not be available in many contexts. Despite their benefits, simulation models face challenges of scalability, data dependency, and generalization. Many struggle to scale up to complex networks or operate under real-time constraints [20,26], and often rely on detailed data inputs such as fragility curves, repair schedules, and demand patterns [25]. Moreover, they are typically calibrated for specific systems, limiting applicability across diverse settings. Few models address the dynamic redistribution of repair resources, a gap also noted by [20].

Recent research (2021–2026) has advanced the field along several complementary directions. At the community scale, the Battle of Post-Disaster Response and Restoration (BPDRR) [28] benchmarked metaheuristic, greedy, and ranking-based restoration strategies on a common earthquake-damaged network under multiple recovery criteria. To cut the cost of stochastic repair-sequence optimization, dynamic importance-ranking heuristics [20,26] and tailored genetic algorithms [29] have been proposed, while learning-based surrogates—graph neural networks and (deep) reinforcement learning—have been introduced to accelerate or replace repeated hydraulic evaluations [30–32]. In parallel, damage modeling has grown more realistic through explicit treatment of spatially correlated pipe damage [33–35] and frameworks that extend beyond pipelines to pumping stations and water treatment plants [36,37]. Whereas these efforts typically optimize restoration for a single damaged network, the present work generalizes recovery assessment into characteristic curves spanning earthquake intensities and repair capacities, coupled with a genetic-algorithm-based optimal repair sequence transferable across networks rather than tailored to a single benchmark instance.

The challenges related to scalability, data dependency, generalization, and resource allocation constraints in current simulation-based recovery models highlight the need for further developments in the field of seismic resilience assessment and recovery planning in WDNs. Addressing these limitations requires models that can not only simulate recovery dynamics but also adapt to diverse scenarios and constrained resources, while simultaneously offering actionable guidance for decision-makers. In response to these challenges, this paper presents a post-earthquake optimization model for WDNs. The primary aim of this model is to identify the optimal pipeline recovery sequence, prioritizing the restoration of critical infrastructure components to enable a faster and more efficient return to full operational capacity. A distinguishing feature of the proposed approach lies in its ability to characterize system behavior under varying levels of seismic stress and repair capacity. By simulating different combinations of these factors, the model generates a series of characteristic curves. These curves, which plot the resilience metric against the recovery rate of the network, offer a comprehensive view of WDN behavior across a spectrum of seismic intensities and resource constraints. As such, they provide valuable insights into the system's capacity to absorb disruptions and recover functionality. In this way, a characteristic curve answers a planning question that a single-scenario repair sequence cannot: for a given hazard level, it identifies how much repair capacity (number of crews) is needed to reach a target resilience and the point beyond which additional capacity stops yielding proportional gains, turning the analysis from a search for "the best sequence for this event" into a tool for sizing recovery resources against the hazard.

The key contributions of this work are the following: (i) Refined surrogate metric for resilience assessment. The study employs a performance-based surrogate metric that enables robust quantification of WDN resilience under seismic conditions; (ii) Post-earthquake optimization model. An optimization model is developed to identify the most effective sequence for pipeline repair, aimed at maximizing system recovery efficiency across varying network topologies and damage scenarios; (iii) Development of characteristic curves. The paper introduces characteristic resilience curves that capture the system's performance under diverse hazard intensities and resource availability levels. These curves enhance the understanding of network adaptability and recovery dynamics; and (iv) Evaluation of resilience for different scenarios. The paper assesses WDN resilience through simulations applied to networks of different scales, providing insight into recovery potential and supporting strategic planning for resource allocation and disaster response.

The remainder of this paper is organized as follows: Section 2 presents the system modeling. Section 3 describes the mathematical formulation of the optimization problem. Section 4 explains the methodology for resilience assessment. Section 5 provides case studies to demonstrate the model's applicability and scalability. Section 6 provides a discussion of the main findings. Finally, Section 7 summarizes the study's conclusions and outlines recommendations for future work.

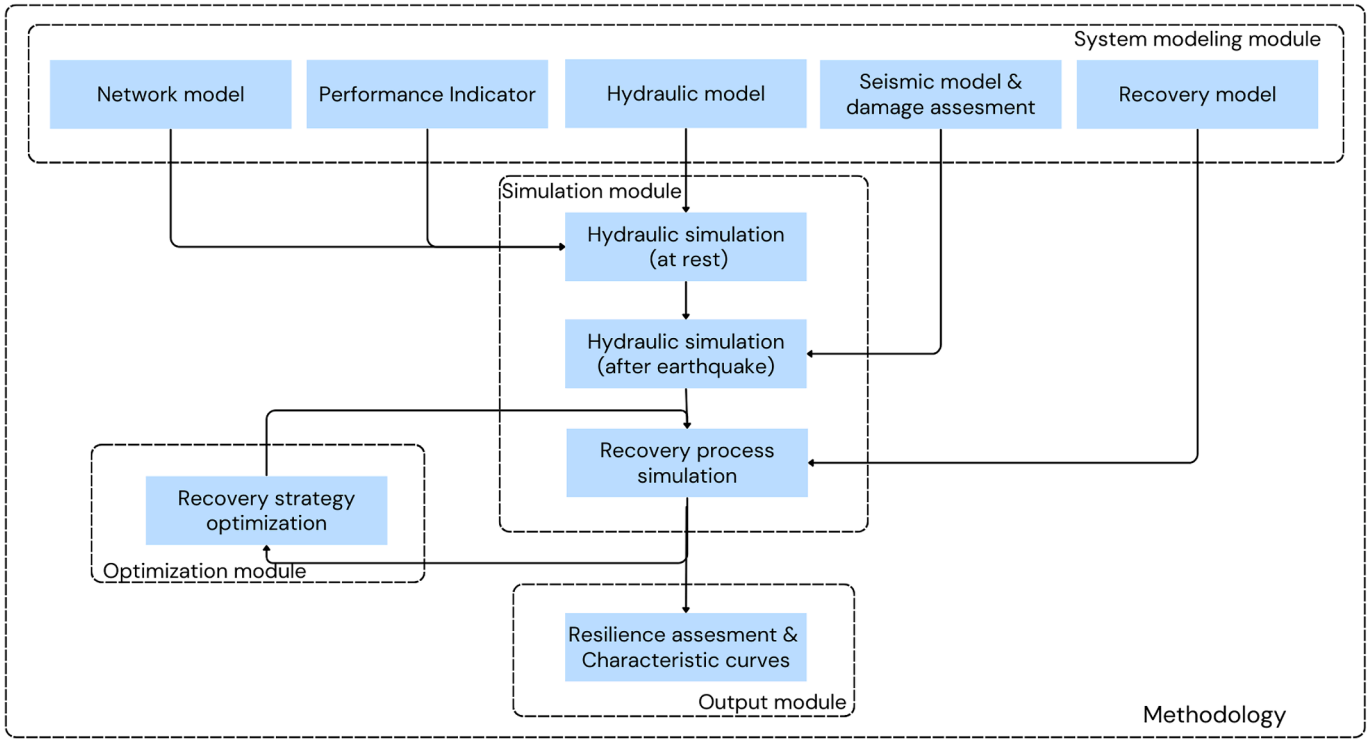

Fig. 1. Overview of the methodology developed for the seismic resilience assessment of WDNs.

2. System modeling

This section outlines the development of each component of the proposed framework, providing the foundation for a comprehensive representation of WDN performance under both normal operating conditions and seismic disruption. Emphasis is placed on capturing the system's behavior during the post-earthquake recovery process. The overall methodology is summarized in Fig. 1, which illustrates the principal steps involved in the seismic resilience assessment. First, the system modeling module defines the basic architecture. It consists of five components that enable modeling the network, assessing system performance, and simulating hydraulic behavior, seismic damage, and the recovery process. The simulation module integrates these components to represent both the initial system behavior and its evolution following the earthquake and throughout the recovery phase. This module is driven by an input recovery strategy. The connections among the elements in Fig. 1 are as follows. The network model, the performance indicator, and the hydraulic model feed the hydraulic simulation of the undisturbed network, which establishes the pre-earthquake baseline heads. The seismic and damage-assessment component then defines the set of damaged pipes, and a second hydraulic simulation of the damaged network quantifies the immediate post-earthquake performance. Both feed the recovery process simulation which, guided by the recovery model (crew capacity and repair logic), reproduces the day-by-day restoration of the network: damaged pipes are progressively restored according to the input recovery strategy and, at each time step of the recovery horizon, the recovery simulation invokes the hydraulic simulation as a subroutine to recompute the nodal heads and evaluate the performance (SDI) of the partially restored network. The optimization module then identifies the optimal recovery strategy, exchanging information with the simulation module in a closed loop: candidate repair sequences are proposed, their simulated performance is returned, and the search iterates until the best-performing sequence is found. Finally, the output module evaluates the system's resilience and generates the characteristic curves. Specific details of each component are provided below.

2.1. Network modeling

The WDN is modeled by incorporating its key components: nodes, pipes, pumps, and valves. The nodes, denoted as $n \in \mathcal{N} = \{1, \ldots, N\}$, include junctions where water is either consumed or redistributed, as well as storage elements such as reservoirs and tanks. While reservoirs maintain a fixed hydraulic head, tanks are characterized by variable water levels depending on their operational role within the system. Pipes, denoted as $i \in \mathcal{P} = \{1, \ldots, P\}$, represent the links that transport water between nodes. For the purpose of this analysis, the modeling process focuses primarily on nodes and pipes, as these components have the most significant influence on the hydraulic behavior and overall performance of the WDN.

Although pumps and valves are included in the hydraulic model to simulate realistic operating conditions, they are excluded from the seismic damage and recovery simulations. This simplification is based on the assumption that such components either experience negligible damage during seismic events or can be repaired and reinstated within a relatively short timeframe [23,26,27]. As such, the analysis centers on pipeline infrastructure as the critical element affecting post-earthquake functionality and system resilience. This is a scoping choice because buried pipelines are the most numerous and frequently governing damage model.

2.2. System performance indicator

The resilience of a WDN is evaluated by assessing its ability to maintain an acceptable level of performance over a time horizon sufficient to complete the post-disruption recovery process. In this context, performance is defined as the system's capacity to satisfy consumer demand under varying operational conditions.

To quantitatively assess the network's functionality during recovery, the Seismic Resilience Index (SRI) is employed. This metric captures the extent to which the network meets user demands throughout the recovery period, and it has been adopted in previous studies on resilience-based recovery modeling [27]. The SRI is calculated as the cumulative

satisfaction of user demand over time, represented by the normalized area under the performance-time curve, as illustrated in Fig. 3. The index is defined as follows:

$$SRI = \frac{1}{T}\sum_{t=1}^{T} SDI(t), \tag{1}$$

where $SDI(t)$ denotes the Satisfaction Degree Index at time step t, reflecting the aggregated performance across all nodes within the network, and T is the recovery horizon. With this normalization, $SRI \in [0, 1]$: a value of 1 corresponds to uninterrupted full service over the entire horizon, so any earthquake-induced loss of service necessarily yields $SRI < 1$. The $SDI(t)$ is computed as:

$$SDI(t) = \sum_{n=1}^{N} w_n \cdot NSD_n(t), \tag{2}$$

where w_n is the weighting factor assigned to each node $n \in N$, indicating its relative importance in the network; the weights can be set, for instance, in proportion to nodal demand or to the importance of the facilities served, so that critical demand nodes, such as those serving hospitals, emergency services, or shelters, are prioritized by assigning them higher weights [38]. The Node Satisfaction Degree $NSD_n(t)$ expresses the level of service at node n at time t, measured as the ratio between the current and pre-disruption hydraulic head:

$$NSD_n(t) = \min\left\{\frac{H_n(t)}{H_n(0)}, 1\right\}. \tag{3}$$

Here, $H_n(t)$ is the hydraulic head at node n at time t, and $H_n(0)$ is the reference head under normal (pre-earthquake) conditions. The use of the minimum function ensures that the satisfaction level is capped at 1.0, preventing overestimation of service restoration in cases where post-recovery pressure exceeds the original value. Nodal satisfaction can alternatively be expressed through delivered outflow, e.g., the ratio of supplied outflow to pre-disruption demand, so that high-demand nodes weigh more than those with little or no demand [12,26]. Two features of the present formulation address this. First, under the pressure-dependent demand model adopted here (Section 2.3), nodal outflow increases with available pressure, so the head ratio in Eq. (3) and the supplied-outflow ratio agree while delivered demand stays below its cap; above the cap, outflow saturates whereas head may keep rising, so they can differ. The head ratio also remains well defined at junctions with little or no demand. Second, the weights w_n in Eq. (2) can be set proportional to nodal demands, prioritizing high-demand nodes as in an outflow-based index; uniform weights are used in the case studies of Section 5. An explicit outflow-based SDI variant would be a direct substitution that leaves the optimization architecture unchanged.

2.3. Hydraulic modeling

The recovery simulation starts with a detailed hydraulic analysis of the WDN in its undisturbed, pre-seismic condition. This initial simulation establishes a baseline for the hydraulic head at each node, which represents the pressure and water availability throughout the system. This baseline is used as a reference to assess the effects of seismic disturbances and the effectiveness of the subsequent recovery strategies, thereby forming a critical foundation for resilience evaluation. This study utilizes the Water Network Tool for Resilience (WNTR), a Python-based package specifically designed for the resilience analysis of water distribution systems [39]. WNTR enables precise hydraulic modeling based on well-established fluid mechanics principles and is fully consistent with industry standards. The tool builds upon the methodology implemented in EPANET 2, a widely accepted software platform for hydraulic and water quality analysis [40], thus ensuring the reliability of the simulation framework. It is noted that, while EPANET 2 itself performs demand-driven analysis, all hydraulic simulations in this study are executed with WNTR's own solver (the WNTRSimulator), which natively implements the pressure-dependent demand formulation described below.

The hydraulic simulation is based on two key principles. First, the conservation of mass is enforced at each network node. Second, the conservation of energy is applied to each link of the network (pipes, pumps, and valves), relating the head difference between its end nodes to the head losses and gains along the link, and accounting for factors such as elevation differences, pipe friction, and pump energy contributions [40]. Water flow through pipes is computed using the Hazen-Williams equation [40], an empirical formula commonly employed for estimating head loss due to friction in pressurized water systems:

$$h_f = k \cdot L \cdot \left(\frac{Q}{C}\right)^{1.852} \tag{4}$$

where h_f is the head loss due to friction, k is a coefficient that depends on the pipe diameter and the unit system, L denotes the length of the pipe, Q is the volumetric flow rate, and C represents the Hazen-Williams roughness coefficient. Higher values of C indicate smoother pipe interiors, resulting in lower head losses. Flow reversals, which may occur when the post-earthquake network topology changes, require no special treatment: as in standard hydraulic solvers, the head-loss term is expressed in the sign-preserving form $h_f \propto |Q|^{0.852} Q$, so that the direction of flow is captured automatically.

To simulate the network's behavior under low-pressure conditions, a pressure-dependent analysis (PDA) is implemented [41]. Unlike demand-driven analysis, which assumes constant node demands irrespective of available pressure, PDA adjusts the delivered demand based on nodal pressure. The actual demand at time t is given by:

$$d(t) = d_{\max} \cdot \min\left(\frac{p(t)}{p_{\min}}, 1\right), \tag{5}$$

where $d_{\max}$ is the nominal maximum demand, $p(t)$ is the pressure at time t, and $p_{\min}$ is the minimum pressure required to fully satisfy the demand.

2.4. Seismic modeling and damage assessment

The subsequent phase of the methodology involves generating a seismic event scenario and evaluating its consequences on the WDN. The seismic event is characterized by its magnitude and the geographical coordinates of its epicenter. To estimate the seismic intensity experienced throughout the network, peak ground acceleration (PGA) and peak ground velocity (PGV) are computed using an attenuation model. These parameters are expressed as functions of the distance from the epicenter to each location within the network.

To quantify the extent of damage to the pipeline infrastructure, fragility curves are utilized in accordance with the procedure described by [5]. These curves provide a probabilistic estimation of the likelihood that a given pipe will reach or exceed a specified damage threshold under particular seismic intensities. In this study, fragility functions are parameterized based on pipe repair rates and lengths, and are used to estimate the probability of failure. For point components, fragility is usually written as a lognormal function of a seismic intensity measure such as PGA or PGV [5]. Pipelines are spatially distributed, so their fragility is expressed instead through the repair-rate model of Eq. (6), which is the form used here.

For simplicity, this study considers two discrete damage states: "No Damage" and "Damage." The "No Damage" condition corresponds to pipelines that maintain full functionality, while the "Damage" state reflects complete functional loss across the entire pipe segment. Minor damages, such as leaks or localized deformations, are excluded from the analysis to maintain a simplified yet conservative modeling approach focused on critical failures. Two states keep the recovery simulation tractable inside the optimization loop, which calls the hydraulic model millions of times, and they match the repair-rate model used below, which predicts how often pipes fail rather than how badly. The two simplifications act in opposite directions. Ignoring minor damage overstates

the performance of lightly damaged networks, while treating moderate damage as a complete loss of the pipe understates it, so the reported resilience and the required repair effort both stay on the safe side. The error is smallest at the magnitudes that govern the characteristic curves, where the failure probability is close to one for almost every pipe (Section 5), and largest at moderate damage levels, where a graded description would leave some pipes partly in service. Section 6 identifies this refinement.

To simulate the spatial distribution of damage, the model samples damage occurrences using the fragility function in conjunction with an exponential distribution [5,42]. This stochastic approach is suitable for representing the random nature of seismic effects on distributed infrastructure. The exponential form follows from treating pipe failures as a Poisson process with rate λ per unit length, the standard damage-occurrence model for buried pipelines [43]. The repair rates themselves are obtained by regressing the number of repairs per unit length observed in past earthquakes on seismic intensity, so the model is fitted to recorded pipe damage. The probability that a pipeline of length L sustains at least one failure is given by the following cumulative distribution function:

$$Prob(S = \text{Damage}) = 1 - e^{-\lambda \cdot L}, \tag{6}$$

where λ is the repair rate dependent on pipe characteristics and seismic intensity, and L is the length of the pipeline. The repair-rate relationships and parameter values adopted here follow established empirical fragility formulations for buried pipelines [43–46]. The rate is taken from the American Lifelines Alliance relation $\lambda = K \cdot 0.00187 \cdot PGV$, with PGV in/s and λ in repairs per 1,000 ft [43]. The correction factor is set to $K = 1$, the reference pipe class of that formulation, because the case-study networks are generic benchmarks for which material, joint, and soil data are not defined. Most corrections for other materials and joints lower λ, so this value stays on the safe side, and for a real network it can be replaced by the tabulated factor or by a regional regression [44,45] without changing the framework. Pipes sampled as undamaged retain their full hydraulic functionality. In contrast, damaged pipes are assumed to be entirely inoperative and are therefore removed from the hydraulic model. This assumption simplifies the repair process by avoiding the need to differentiate between various levels of pipeline impairment. Treating damaged pipes as fully out of service implicitly assumes that failures are detected promptly after the event and that the affected pipes can be isolated from the rest of the network, for instance through isolation valves at their ends. The alternative is to represent damaged pipes as highly leaking elements with pressure-dependent discharge, as adopted in the Battle of Post-Disaster Response and Restoration [28] and related studies [47]; this refinement, which requires calibrated leak-area data, is identified as an extension in Section 6.

The outcome of the damage sampling defines what is referred to in the remainder of this paper as the *damage level* of the network: the set of damaged pipes, and the corresponding total damaged length, generated for a given earthquake magnitude (higher magnitudes yield higher damage levels). Consistent with the two-state damage model, a damaged pipe is treated as a single repair intervention covering its entire length, representing the combined effort of locating and repairing the possibly multiple breaks along the pipe and of inspecting and recommissioning it; in practice, earthquake damage concentrates at discrete locations along the pipeline, and modeling point repairs of individual breaks is a further refinement (Section 6).

Finally, because damage states are sampled from probability distributions, a given earthquake magnitude can produce different damage realizations. In the case studies of Section 5, one fixed realization per magnitude is generated with a single random seed, so that comparisons across magnitudes and repair capacities are not confounded by sampling noise.

The exclusion of damaged pipes from the hydraulic network modifies its topology and introduces new constraints, such as increased head losses and reduced redundancy. These changes affect the overall hydraulic performance of the system. To reflect these changes, a hydraulic simulation is conducted using the reconfigured network. The simulation adheres to the conservation principles outlined previously and updates nodal hydraulic heads to capture the network's degraded performance state. The resulting SDI quantifies the immediate impact of the earthquake, serving as a basis for evaluating the post-damage system condition.

2.5. Recovery modeling

The recovery process for the WDN starts immediately after the seismic event takes place, which is designated as day 0 in the simulation. The repair operations continue over a time horizon of T days. The duration T corresponds to the time required to achieve full system restoration for a specific earthquake magnitude and available repair rate. By definition, T does not exceed the maximum recovery period $T_{\max}$, which is determined as the number of days needed to repair the network under the most severe scenario, characterized by the highest magnitude and the lowest available repair capacity.

The recovery process is governed by a repair sequence vector, denoted by $\mathbf{X}$, which specifies the order in which damaged pipes are to be restored. Formally, $\mathbf{X}$ is a one-dimensional vector of length D, where $D \leq P$, with P representing the total number of pipes in the network. Each element x_i in $\mathbf{X} = [x_1, x_2, \ldots, x_D]$ indicates the repair order of the i-th damaged pipe.

Repairs are conducted by crews operating at a fixed repair rate R, defined as the length of pipe that can be restored per day. This rate reflects the daily repair capacity of the available workforce and equipment. The crews are assumed to be fully mobilized at the onset of the recovery phase, and repairs are treated as non-preemptive. That is, once the repair of a given pipe begins, it must be completed before the crew proceeds to the next pipe in the sequence. When multiple crews are available, they are not dispatched individually to different pipes; instead, the workforce is modeled as a single aggregate repair capacity, with R scaling proportionally with the number of crews. The crews thus work jointly on the same pipe, restoring damaged pipes one at a time in the order specified by $\mathbf{X}$; any capacity left over on the day a pipe is completed is immediately reallocated to the next pipe in the sequence. Explicit scheduling of crews operating in parallel on different pipes is identified as an extension in Section 6. The repair duration of each damage follows directly: it equals the pipe length divided by the daily repair capacity R, after accounting for the capacity already committed to preceding pipes. Repair durations are therefore deterministic for a given damage scenario, so the recovery-time uncertainty originates from the stochastic damage scenario sampled through the fragility model, while crew-productivity uncertainty is addressed parametrically, by evaluating the recovery across a wide range of repair rates when constructing the characteristic curves (Section 4).

To simulate this process, the sequence vector $\mathbf{X}$ is transformed into a matrix $\bar{\mathbf{X}}$, which tracks the repair status of each pipe over time. This matrix has dimensions $P \times (T_{\max}/\Delta t)$, where $\Delta t = 1$ day, consistent with the daily resolution of the recovery simulation. The matrix transformation is necessary because $\mathbf{X}$ encodes only the repair order, whereas $\bar{\mathbf{X}}$ captures the dynamic progression of pipe repairs throughout the recovery period.

Each entry $\bar{X}_{it}$ in the matrix denotes the proportion of pipe i that remains unrepaired on day t. Initially, all damaged pipes are marked as fully damaged:

$$\bar{X}_{it} = 1, \quad \forall i \in \mathcal{D}, \forall t \in \{1, \ldots, T_{\max}\}. \tag{7}$$

where $\mathcal{D}$ is the subset of damaged pipes. At the beginning of each day, the available repair capacity is set to the predefined value R. The remaining unrepaired length of the current pipe, denoted as J_i, is compared to the available capacity. If $J_i \leq R$, the pipe is fully repaired that day, and the entry $\bar{X}_{it}$ is updated to zero, indicating the restoration of the pipe.

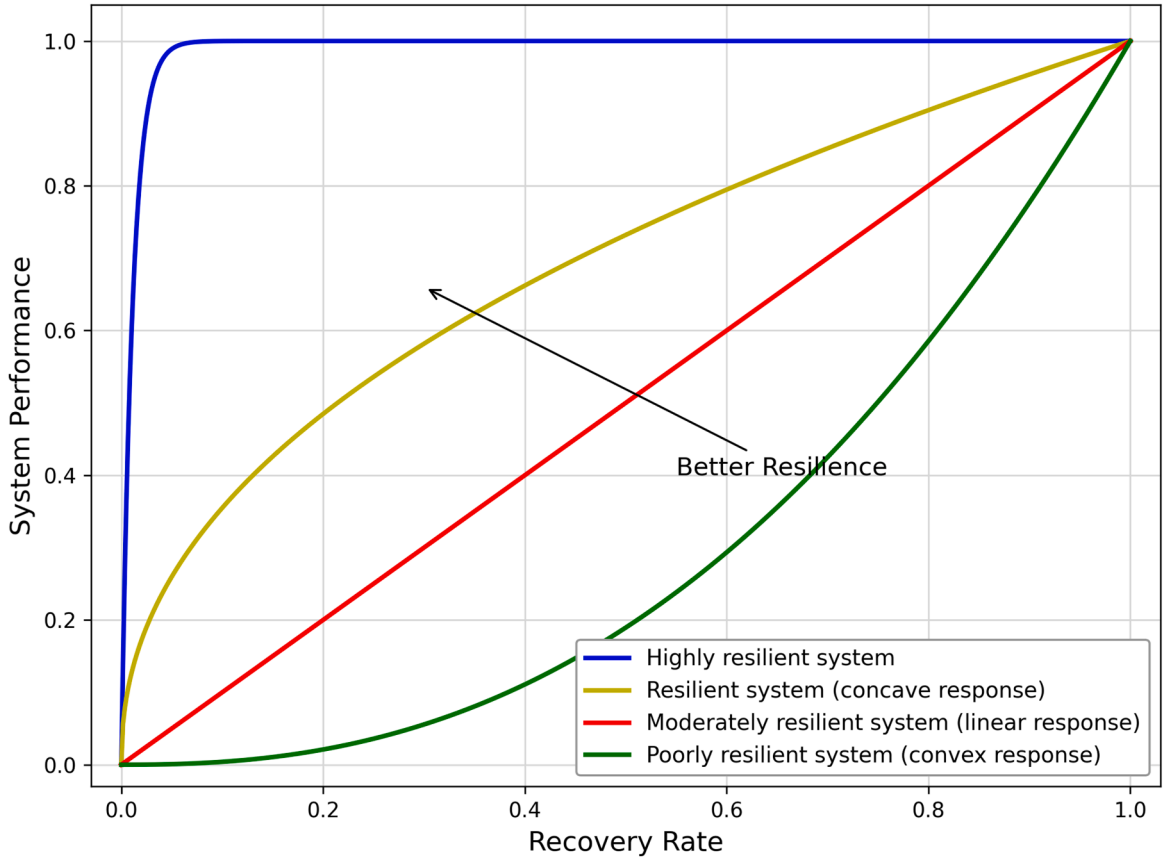

Fig. 2. Example of characteristic curves depicting the system's recovery capacity for systems with different resilience characteristics. Curves closer to the upper-left corner correspond to systems that reach high performance at lower recovery rates, i.e., better resilience.

The remaining repair capacity is then adjusted to reflect the completed repair.

If $J_i > R$, only a partial repair is completed, with a length equal to the remaining daily repair capacity. The matrix $\bar{X}_{ii}$ is updated to reflect the remaining unrepaired portion of the pipe. In this case, the daily repair capacity is fully expended, and repair of the pipe continues on the subsequent day. This process repeats until either all damaged pipes have been addressed or the daily capacity is exhausted.

At the conclusion of each day, a hydraulic simulation is performed to reflect the evolving state of the network. This simulation updates the hydraulic head at each node, accounting for the improved functionality resulting from completed repairs. Following this, the SDI is recalculated, providing a dynamic measure of the network's operational performance as the recovery progresses. This iterative process continues until all damaged components are fully restored or the recovery period elapses.

3. Recovery strategy optimization

This section presents the mathematical formulation of the proposed optimization model, which is designed to determine the most effective recovery strategy for a WDN following a seismic event. The primary objective is to enhance network resilience by identifying the optimal sequence in which damaged pipelines should be repaired.

The recovery process is represented by the vector $\mathbf{X} = [x_1, x_2, \ldots, x_D]$, where each element x_i corresponds to the repair priority assigned to the i-th damaged pipe. Each variable x_i is an integer within the interval $[0, D]$, with D denoting the total number of damaged pipes.

The objective of the optimization model is to maximize the seismic resilience of the network by minimizing the negative of the time-weighted SDI over the recovery period T. The objective function is formulated as:

$$\min_{\mathbf{X}} -\sum_{t=1}^{T} \frac{SDI_t(\mathbf{X})}{t}. \tag{8}$$

This formulation incorporates a temporal penalty that prioritizes early restoration. By assigning greater weight to earlier time steps, the model favors recovery strategies that restore functionality more rapidly. Such prioritization is consistent with the concept of resilience, which emphasizes swift performance recovery following a disturbance. As illustrated in Fig. 2, strategies yielding higher resilience curves-represented by a greater area under the curve-are preferred. This demand-satisfaction-based, time-weighted objective builds on resilience metrics adopted and verified in previous recovery-optimization studies [26,27]; the resulting sequences are benchmarked in Section 5 against demand- and head-based prioritization strategies, which are standard importance-ranking baselines in WDN restoration [20,26], and a systematic comparison with dynamic importance-ranking and learning-based solvers is identified as future work (Section 6).

The optimization problem is subject to the following constraints:

(1) Order constraint: The repair assignment must fall within the valid range of damaged pipes:

$$0 \le x_i \le D, \quad \forall i \in \mathcal{D} \tag{9}$$

This constraint ensures that repairs are scheduled exclusively for the damaged subset of pipes $\mathcal{D} \subseteq \mathcal{P}$, thereby excluding undamaged components from the recovery sequence.

(2) Permutation constraint: Each damaged pipe must be repaired exactly once, and the repair order must be unique:

$$x_i \neq x_j, \quad \forall i \neq j, \quad i, j \in \mathcal{D} \tag{10}$$

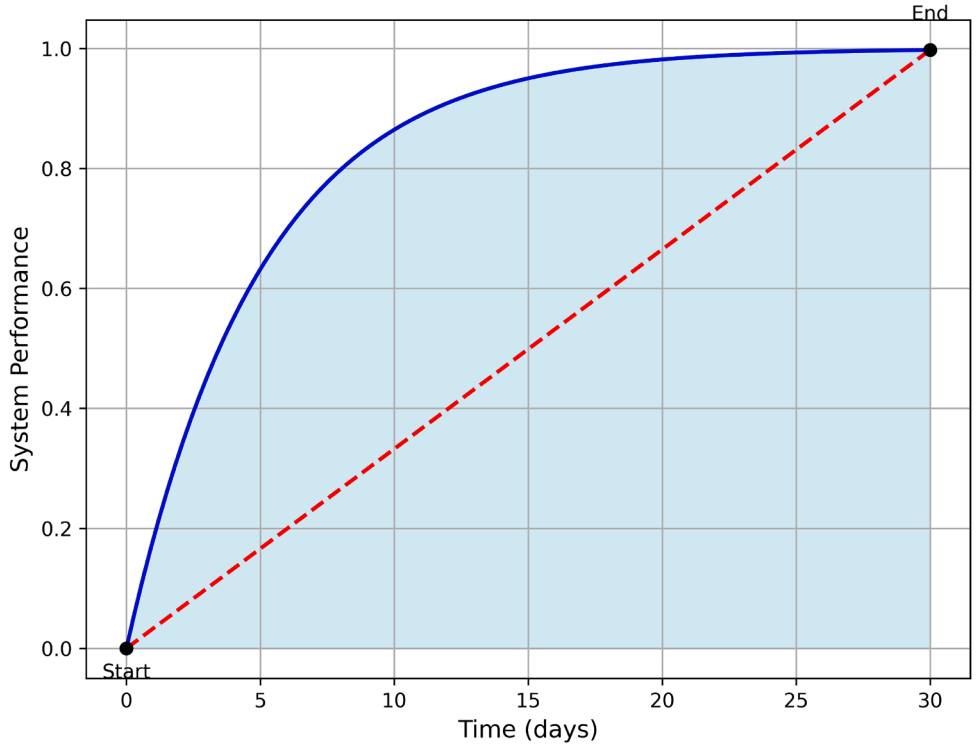

Fig. 3. Resilience curve illustrating the repair rate as the secant of the SDI curve.

This constraint prevents any duplication in the repair schedule and ensures that each repair action is executed precisely once, thereby reflecting operational feasibility and avoiding redundant actions.

For reference, the hydraulic head at a node is considered adequate for normal service when it lies within the range

$$H_{\min} \le H_{n,t}(\mathbf{X}) \le H_{\max}, \quad \forall n \in \mathcal{N}, \forall t \in \{1, \dots, T\} \tag{11}$$

which is shown for reference only and is not imposed neither as a constraint nor as a target. The optimization places no constraint on the hydraulic head; under the pressure-dependent model, pressures below the requirement reduce the delivered demand (Eq. (5)), a loss of service that the objective already captures.

3.1. solution approach: Genetic algorithm

Given the combinatorial nature of the problem in which the optimal repair schedule must be selected among the $D!$ possible permutations of the damaged pipes, the optimization is solved with a Genetic Algorithm (GA), a metaheuristic well suited to sequencing problems of this type that has been widely applied to post-disaster recovery optimization of WDNs [27,29]. The implementation relies on the open-source library PyGAD [48].

Each candidate solution (chromosome) is encoded as a vector of D integer genes, one gene per damaged pipe, where the value of the i-th gene defines the repair priority of the i-th damaged pipe. A chromosome is thus a permutation of the D repair priorities, satisfying the order and permutation constraints of Eqs. (9) and (10); duplicate gene values are automatically resolved by the GA operators, so that crossover and mutation always return valid permutations. The number of genes equals the number of damaged pipes in the scenario at hand.

The simulation module evaluates a candidate sequence as follows: (i) the damaged pipes are removed from service in the WNTR network model; (ii) the recovery model decodes the sequence, determining day by day the repair progress and the day each pipe returns to service, given the daily repair capacity R; (iii) at each pipe restoration, the pressure-dependent hydraulic simulation (Section 2) is re-run on the updated network to obtain nodal heads, from which $NSD_n(t)$ and $SDI(t)$ are computed at each daily step of the recovery horizon; and (iv) the time-weighted objective of Eq. (8) is returned to the GA as the candidate's fitness. The GA evolves a population of 100 sequences using steady-state parent selection (5 mating parents, the 2 best retained in the next generation), single-point crossover (probability 0.99), and random mutation (probability 0.05, affecting up to 10% of the genes). The number of generations is set per case, with convergence behavior shown in Section 5.

As a low-cost benchmark for the GA, we also consider the dynamic importance (DI) ranking heuristic of [20,26], widely adopted for post-earthquake repair sequencing. Rather than searching the permutation space, DI ranking builds the sequence greedily: at each step it restores the not-yet-repaired pipe whose immediate restoration yields the largest gain in system SDI, re-evaluating this importance after every repair so the ranking reflects the evolving hydraulic state of the partially restored network. The heuristic is deterministic and uses the *identical* hydraulic, recovery, and SDI/SRI module as the GA, so the two solvers differ only in how the repair sequence is built. Its cost is of order D^2 hydraulic evaluations ($D(D+1)/2$ for the greedy search plus two diagnostic baseline solves), against the GA's $N_{\text{pop}}\,(N_{\text{gen}}+1)\,D$.

4. Resilience assessment & characteristic curves

This section outlines the method used to assess the resilience of the WDN following the recovery process, based on the near-optimal repair sequence. To evaluate the system's overall performance, the recovery strategy is examined across a range of scenarios defined by varying earthquake intensities and different repair crew capabilities.

For each scenario, the SRI is calculated using the SDI values over the full recovery period. Resilience is thus quantified explicitly by the SRI of Eq. (1), i.e., the time average of the SDI over the recovery horizon, equivalent to the normalized area under the performance–time curve. These values are then used to construct characteristic curves, which visually represent the relationship between network resilience and repair rates. Arango et al. [49] proposed the characteristic curves for the first time, using them to characterize the recovery capacity of road

networks following wildfires. This paper extends this concept to water supply networks following earthquakes. The construction of the curve does not depend on the hazard that caused the damage, since it relates a resilience metric to the repair capacity and needs only a damage scenario, a recovery model, and a performance indicator. What changes for earthquakes are these three ingredients, built here from seismic attenuation, pipeline fragility, and pressure-dependent hydraulics (Sections 2.4 and 3). The curves assume that all damage occurs at the start and that performance only improves during recovery, so events that damage the network again while it is being repaired, such as strong aftershocks, fall outside their scope.

As illustrated in Fig. 2, an optimal recovery strategy is one that achieves high performance with the lowest feasible repair rate. The development of characteristic curves consists of two main components: the performance matrix for the selected resilience metric, and the associated recovery rate.

The performance matrix is constructed from SDI values, which capture the WDN's functional status at each time-step t according to Eq. (2). These values are generated based on the optimal repair sequence applied under different seismic intensity levels. Each row of the matrix corresponds to a distinct damage level $m \in \{1, \dots, M\}$ (i.e., the damage scenario generated for the m-th earthquake magnitude, as defined in Section 2.4), while each column denotes a discrete time-step t, resulting in a two-dimensional representation of performance over time and across hazard scenarios.

The average network performance at a given hazard level is obtained by computing the mean of the SDI values over the full recovery duration, denoted as $T_{\max}$. This ensures that the performance matrix reflects the temporal dynamics of the system under the most adverse conditions. The matrix is expressed as:

$$SDI_{m,t} = \begin{bmatrix} \mathrm{SDI}(1,1) & \mathrm{SDI}(1,2) & \dots & \mathrm{SDI}(1,T_{\max}) \\ \mathrm{SDI}(2,1) & \mathrm{SDI}(2,2) & \dots & \mathrm{SDI}(2,T_{\max}) \\ \vdots & \vdots & \ddots & \vdots \\ \mathrm{SDI}(M,1) & \mathrm{SDI}(M,2) & \dots & \mathrm{SDI}(M,T_{\max}) \end{bmatrix} \tag{12}$$

This formulation enables the representation of system recovery performance for each damage level across time, forming the basis for generating characteristic resilience curves.

In parallel, the recovery rate is defined as the average hydraulic head restored across the entire network per unit of time and is expressed in m/day. This is computed as the secant of the SDI curve for each pair of damage level and repair rate, serving as a quantitative measure of recovery efficiency.

Fig. 3 illustrates a typical resilience curve, where the slope of the secant line represents the recovery rate. This representation allows for the comparison of different scenarios with varying levels of damage and repair resources, thereby facilitating an evaluation of trade-offs between repair capacity and system performance.

The resulting characteristic curves are valuable tools for decision-makers, as they provide insights into how the WDN responds to different stress levels and recovery capacities. They enable the identification of critical thresholds beyond which additional repair resources significantly improve recovery outcomes. Moreover, these curves emphasize the importance of strategic resource allocation and planning, particularly in scenarios where limited resources must be deployed effectively to restore service and mitigate post-disaster impacts.

5. Application cases

To illustrate the applicability of the proposed model, this section presents its implementation across two distinct case studies involving different WDNs. The first case study is based on a standardized benchmark network that is frequently used for the evaluation of WDN performance. The second case study involves a scalable network designed to approximate the structural and operational characteristics of a small real-world urban water distribution system.

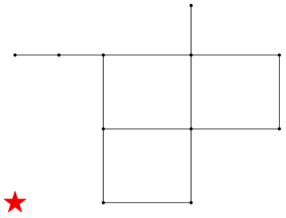

Fig. 4. Illustration of Network 1 from the EPANET example set and the location of the epicenter of the earthquake.

Table 1
Pipe names and corresponding lengths for Network 1 (rounded to the nearest 0.1 km; the network totals approximately 19.1 km).

Pipe IDs	Length (km)
10	3.2
1	0.8
12	1.6
21	1.6
22	0.7
31	0.6
110	0.6
111	2.1
112	0.8
113	3.0
121	3.0
122	0.9

5.1. Case 1

5.1.1. Case description

The first case study is based on a modified version of Network 1 from the EPANET example set, developed by the United States Environmental Protection Agency (EPA).

As shown in Fig. 4, this network consists of 12 pipes, 9 junctions, 1 pump, 1 tank, and 1 reservoir. The demand at each junction follows a 24 h pattern, which captures the daily variability in water consumption. To enhance the relevance of the case study, minor modifications were applied to the original pipe lengths. These modifications were intended to introduce greater variability, as the initial network included groups of pipes with uniform lengths. This adjustment was made to prevent premature convergence of the optimization algorithm toward suboptimal solutions influenced by uniform pipe characteristics. The total pipeline length of the modified network is 19 km. Table 1 presents the identifiers and respective lengths of all pipes in the network.

The seismic event is assumed to originate at the bottom-left corner of the network, as indicated in Fig. 4. Earthquake magnitudes ranging from 6.0 Mw to 9.0 Mw were simulated to investigate the resulting damage under varying hazard intensities. Fig. 5 shows the relation between earthquake magnitude and the extent of pipe damage, both in terms of total broken length and number of affected pipes.

5.1.2. Optimal recovery strategy

The recovery strategy is obtained using the optimization problem outlined in Section 3. The optimization has been solved using a Genetic Algorithm (GA), with the settings reported in Section 3.1: a population of 100 candidate sequences, steady-state parent selection with 5 mating parents and 2 parents retained per generation, single-point crossover with probability 0.99, and random mutation with probability 0.05 (affecting up to 10% of the genes). The number of generations was set to 30 for this case, which proved ample for convergence (Fig. 7). This subsection presents the results for a high-severity scenario in which the earthquake magnitude reaches 9.0 Mw, and only a single repair crew is

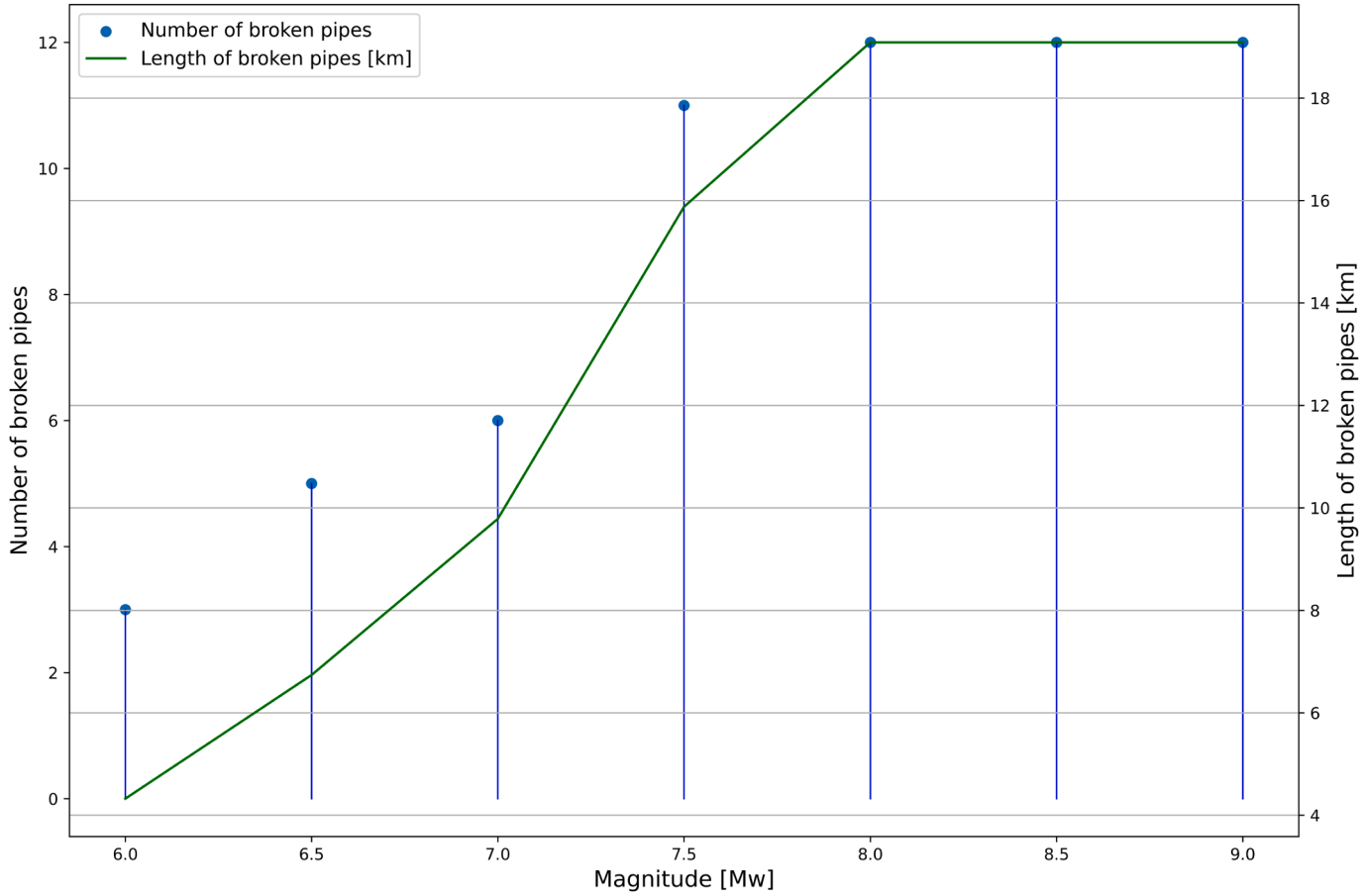

Fig. 5. Number and length of broken pipes versus earthquake magnitudes for Network 1.

available, operating at a constrained repair rate of 25 m/day. The crew repair-rate values considered in the case studies (25–150 m/day, corresponding to one to six crews) are representative values chosen to span a realistic range of crew productivity, consistent with restoration data reported for buried water pipelines [43].

To evaluate the performance of the proposed approach, the optimized recovery sequence derived by the GA is compared against two baseline prioritization strategies. The first strategy ranks the pipes based on the average water demand at their start and end nodes, with higher priority assigned to those associated with greater demand. The second strategy ranks the pipes according to the average hydraulic head at the connecting nodes, thereby giving precedence to pipelines that potentially convey higher pressure. Both are *static* importance-ranking baselines: each pipe is ranked once, by a fixed attribute (its nodal demand or head, computed before recovery), and this ranking is not updated as repairs proceed—in contrast to the *dynamic* importance (DI) ranking of Section 3.1, which re-evaluates pipe importance after every repair.

Fig. 6 presents the trajectories of the SDI for all three recovery strategies. Each discrete step in the curves represents the completion of an individual pipe repair. The GA-optimized strategy (red curve) demonstrates a faster rate of recovery and achieves a final SRI of 0.831. In contrast, the head-based strategy (blue) results in an SRI of 0.536, while the demand-based strategy (yellow) achieves an SRI of only 0.255.

Although perfect resilience ($SRI = 1$) is not reached under this constrained scenario, the GA-based strategy restores 90% of the SDI within the first year, during which 9 out of the 12 damaged pipes are fully repaired. This indicates that the GA prioritizes repairs that maximize early-stage gains in network functionality. Two clarifications are due. First, recovery duration follows from the damage volume and the available repair capacity: under the 9.0 Mw scenario the fixed damage realization breaks all 12 pipes of Network 1, totaling about 19.1 km, so a single crew at 25 m/day needs roughly 764 days for full restoration, whereas six crews (150 m/day) clear the same damage in about 127 days. Although Network 1 is topologically small, its pipes are long trunk lines (about 0.6 to 3.2 km), and recovery time is governed by the damaged length divided by the repair capacity rather than by the number of pipes. Second, the network returns to its pre-earthquake performance: the SDI reaches 1.0 once all pipes are repaired (Fig. 6). The SRI, by contrast, is cumulative, calculated as the time-averaged SDI over the recovery horizon, Eq. (1), so service lost while the network was degraded cannot be recovered afterwards, and $SRI = 1$ is attainable only without any disruption.

A sensitivity check on Network 1 (20 random realizations per magnitude) shows that the damage extent is essentially saturated at the high intensities governing the worst-case characteristic curves (all 12 pipes, about 19.1 km, at 9.0 Mw, with negligible scenario-to-scenario variability) whereas moderate intensities show appreciable spread (for example about 6.8 ± 1.4 of the 12 pipes, about 13.4 km, at 7.0 Mw); the fixed realization is therefore representative of the high-magnitude regime emphasized here. Evaluating full ensembles to endow the characteristic curves with confidence bands across all intensities is identified as a refinement (Section 6).

The recovery curve corresponding to the optimal sequence exhibits a steep initial rise, followed by a more gradual improvement. This pattern reflects the algorithm's ability to identify and prioritize critical infrastructure components early in the recovery process. In contrast, the fixed-order strategies exhibit suboptimal recovery behaviors. The ordering visible in Fig. 6, that is, the optimal sequence (red) above the head-based ranking (blue), itself above the demand-based ranking (yellow), has a clear hydraulic interpretation: the GA explicitly searches for the

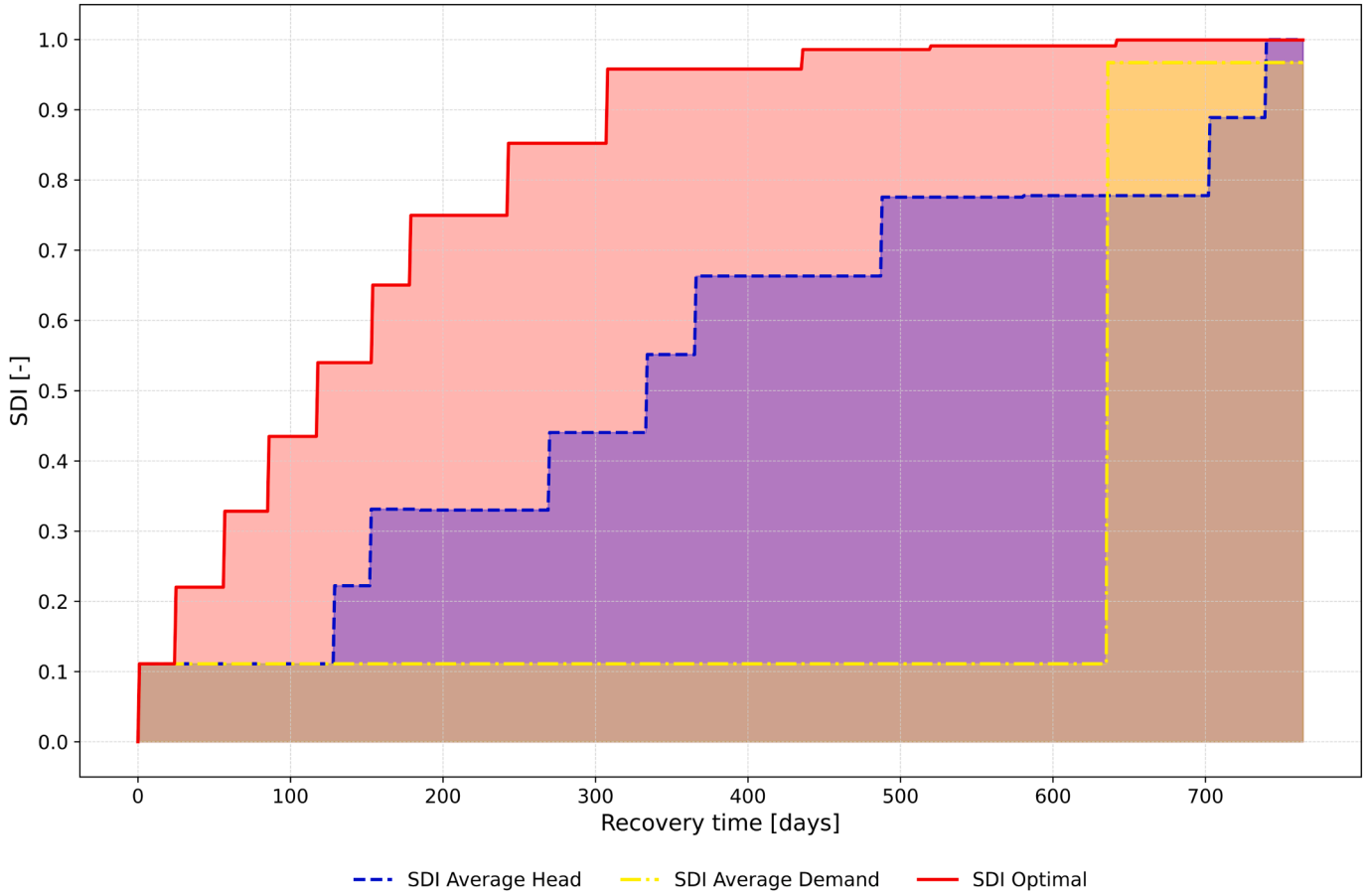

Fig. 6. SDI curve for Network 1 for the optimal recovery sequence and for the fixed strategies.

sequence that maximizes early gains in delivered service; the head-based ranking happens to restore the high-pressure transmission paths relatively early; and the demand-based ranking repairs pipes whose downstream nodes remain disconnected from the sources for most of the recovery, so that their repair yields little immediate benefit.

The demand-based approach fails to consider network connectivity. As a result, many of the repaired pipes do not immediately contribute to improved hydraulic performance. This is evident from the near-flat portion of the SDI trajectory, where only upon repairing nearly all pipes does the system begin to recover significantly.

The head-based strategy yields moderately better results. This is expected, given that hydraulic head influences the driving pressure within the system. However, it still lacks a mechanism to exploit network redundancy. By prioritizing pipes with high head values indiscriminately, it fails to identify the minimal set of critical components required for early restoration. Consequently, the recovery is slower and the overall resilience is reduced, as reflected in the lower SRI.

To examine the behavior of the Genetic Algorithm throughout the optimization process, the box-plot in Fig. 7 illustrates the progression of solution quality across generations during the search process. During the initial stages, the interquartile range is wide, indicating extensive exploration of the solution space. This diversity in early generations promotes the identification of high-quality solutions.

By generation 14, the range of solution fitness narrows significantly, indicating convergence towards high-performing recovery sequences. Complete convergence is achieved by generation 17, at which point the variability across the population becomes minimal.

The presence of outliers in the later generations reflects the GA's continued exploration, even after convergence. These outliers correspond to alternative recovery sequences, which help to maintain genetic diversity within the population. However, their negligible impact on the best fitness values suggests that the algorithm consistently identifies near-optimal solutions. This demonstrates the robustness of the optimization approach and its ability to balance exploration with convergence effectively.

5.1.3. Characteristic curves

This subsection presents the characteristic curves for Network 1, which illustrate the restorative performance of the system under varying levels of seismic intensity and repair capacity.

Fig. 8 shows the SRI achieved by the network over the course of the recovery process, based on the optimal recovery sequence. The results are expressed as a function of the recovery rate, defined as the average hydraulic performance regained per unit of time during the recovery period. Each curve corresponds to a specific number of repair crews, with associated repair rates ranging from 25 m/day (1 crew) to 150 m/day (6 crews). Individual points along the curves represent increasing earthquake magnitudes, from 6.0 Mw (top of each curve) to 9.0 Mw (bottom).

Several notable trends emerge from the analysis. For low earthquake magnitudes (e.g., 6.0 Mw), the network demonstrates full recovery ($SRI = 1$) across all repair rates. However, for more severe seismic events (e.g., 9.0 Mw), network resilience is constrained by the available repair resources. For instance, at the lowest repair rate (25 m/day), the network achieves an SRI of only 0.810, indicating incomplete recovery due to extended restoration time. As the repair rate increases, the corresponding SRI improves, reaching a maximum of 0.970 at 150 m/day. Nevertheless, this value still falls short of full resilience, suggesting that even the highest resource allocation is insufficient to guarantee complete restoration under extreme damage scenarios.

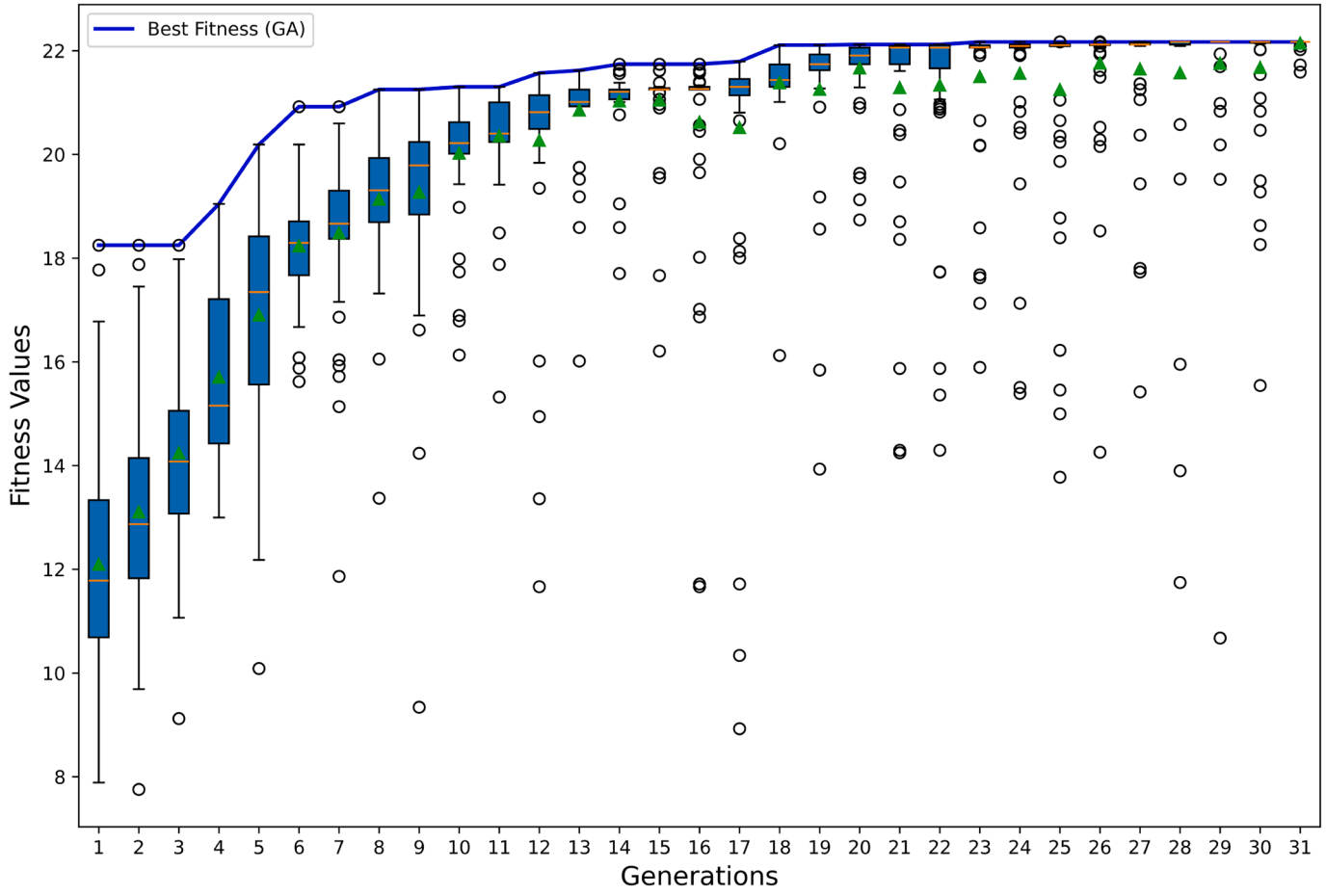

Fig. 7. Box-plot of the results of the GA search for Network 1. For each generation, the box spans the interquartile range of the population fitness, the orange line marks the median, the green triangle the mean, the whiskers extend to the non-outlier range, and the open circles denote outliers; the blue line tracks the best fitness found up to each generation.

The relationship between repair capacity and recovery rate is found to be linear for low-to-moderate earthquake magnitudes. This indicates that increases in available resources lead directly to proportional improvements in recovery efficiency. By contrast, for higher magnitudes, this linearity diminishes. For example, while increasing the repair rate sixfold (from 25 to 150 m/day) yields substantial benefits at 6.0 Mw, the same increase results in only marginal gains at 9.0 Mw. This nonlinear response highlights the diminishing returns associated with scaling resource availability under severe damage conditions.

This behavior can be attributed to the network topology and the requirement to first restore critical pathways before functionality can be re-established. In such cases, even with increased repair capacity, early repairs may not immediately result in performance gains, as multiple interdependent components must be repaired before flow continuity is achieved. This phenomenon is reflected in the slower recovery rates observed under high-damage scenarios.

Moreover, the results indicate that at lower repair rates, such as 25 m/day, the average recovery rate remains low (approximately 0.005 m/day), emphasizing the need for additional resources to avoid prolonged service disruptions. Conversely, while higher repair rates (e.g., 150 m/day) lead to faster recovery, decision-makers must weigh the associated costs against the marginal benefits in resilience. The characteristic curves suggest that for severe hazard scenarios, allocating greater resources does not necessarily translate into proportional gains in performance. This observation implies that a more strategic deployment of resources may be required to improve the cost-effectiveness of the recovery process.

Fig. 9 presents a complementary perspective by examining the influence of seismic magnitude on the recovery behavior. In this case, SRI is plotted as a function of recovery rate for earthquakes ranging from 6.0 Mw to 9.0 Mw.

The figure highlights how the initial damage level, governed by earthquake magnitude, influences the achievable resilience. For 6.0 Mw, the initial damage is minimal, resulting in high SRI values and fast recovery regardless of repair rate. As seismic intensity increases, recovery becomes increasingly dependent on both the severity of the disruption and the availability of resources.

Notably, the response of the network to different magnitudes can be categorized into three behavioral clusters. For magnitudes of 6.0 Mw, the network is largely unaffected and achieves near-full recovery with minimal intervention. For magnitudes between 6.5 and 7.0 Mw, minor disruptions are observed, with sufficient recovery achievable using moderate resources (e.g., three repair crews). However, for magnitudes exceeding 7.5 Mw, the extent of damage becomes substantial, and the available repair resources are no longer sufficient to ensure complete recovery. In these cases, the recovery rate becomes constrained by the number of critical components that must be restored before performance improvements are realized.

The recovery trajectories for these higher magnitude events display flatter slopes, reflecting a slower restoration process despite increased repair rates. These results emphasize the importance of pre-disaster

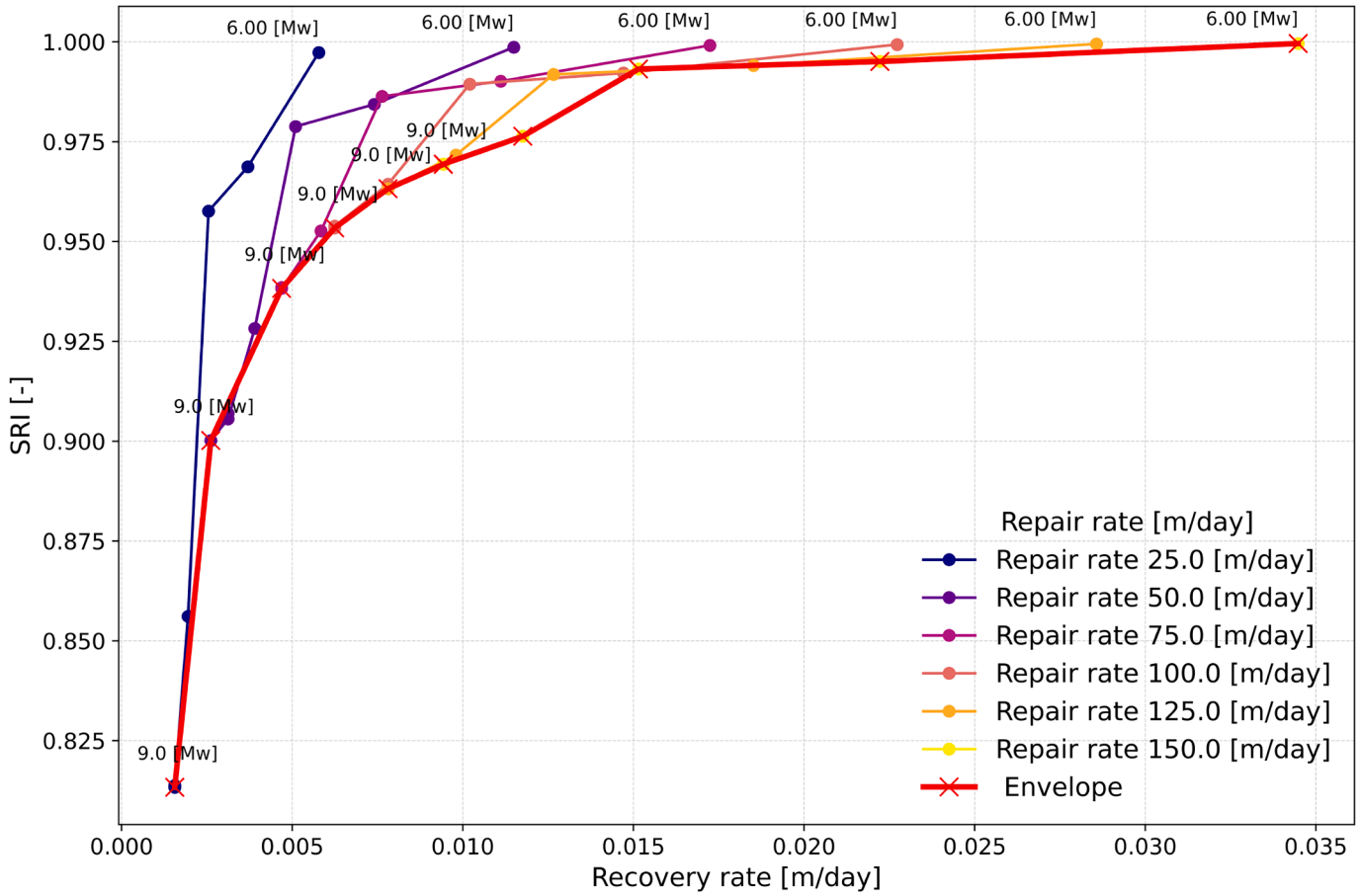

Fig. 8. Characteristic curves of SRI as a function of recovery rate for varying repair rates in Network 1.

Table 2
Pipe names and corresponding lengths for Network 3. A complete list is available in the Appendix.

Pipe IDs	Length (km)
20	0.03
40	0.03
50	0.03
60	0.3
101	4.3
103	0.4
105	0.7
109	1.2
111	0.6
…	…
330	3.0
333	0.9

planning and strategic resource allocation, particularly for regions vulnerable to high-magnitude seismic activity.

5.2. Case 2

5.2.1. Case description

The second case study focuses on Network 3 from the EPANET example set, developed by the U.S. Environmental Protection Agency (EPA).

Network 3 is based on the North Marin Water District (NMWD) located in Novato, California. This district serves an estimated population of 64,000 across a geographic area of approximately 100 mi^2. The network represents a significantly larger and more complex system compared to Network 1, comprising 118 pipes, 92 junction nodes, 2 pumping stations, 3 storage tanks, and 2 constant-head reservoirs, as illustrated in Fig. 10.

Originally developed as part of a water quality investigation [50], this network is characterized by both operational and structural diversity. The nodes follow a 24 h demand pattern, consistent with that used in Case 1 (Section 5.1). The total pipeline length across the 118 pipes is approximately 150 km. Table 2 presents a representative sample of the pipe lengths, while the full dataset is provided in the Appendix for reference.

To assess the seismic vulnerability of the network, earthquake magnitudes ranging from 6.0 Mw to 9.0 Mw were simulated. The epicenter of the earthquake was assumed to be located in the upper left corner of the network. The number of broken pipes and total length of pipeline damage were recorded for each magnitude, as shown in Fig. 11.

5.2.2. Optimal recovery strategy

This section analyzes the recovery performance of Network 3 under various resource availability scenarios, with a particular focus on the most vulnerable condition: a seismic event of magnitude 9.0 Mw and a single available repair crew operating at a daily repair rate of 25 m/day. Fig. 12 presents the hydraulic performance recovery curves, measured using the SDI, comparing the near-optimal recovery strategy-produced by the GA-against two baseline strategies: one based on average hydraulic head and the other on average node demand.

The results indicate that the near-optimal strategy significantly outperforms both baselines, achieving an SRI of 0.698. This value reflects the system's reduced resilience under limited resources but remains a substantial improvement over the average head-based strategy ($SRI = 0.372$) and the average demand-based strategy ($SRI = 0.272$).

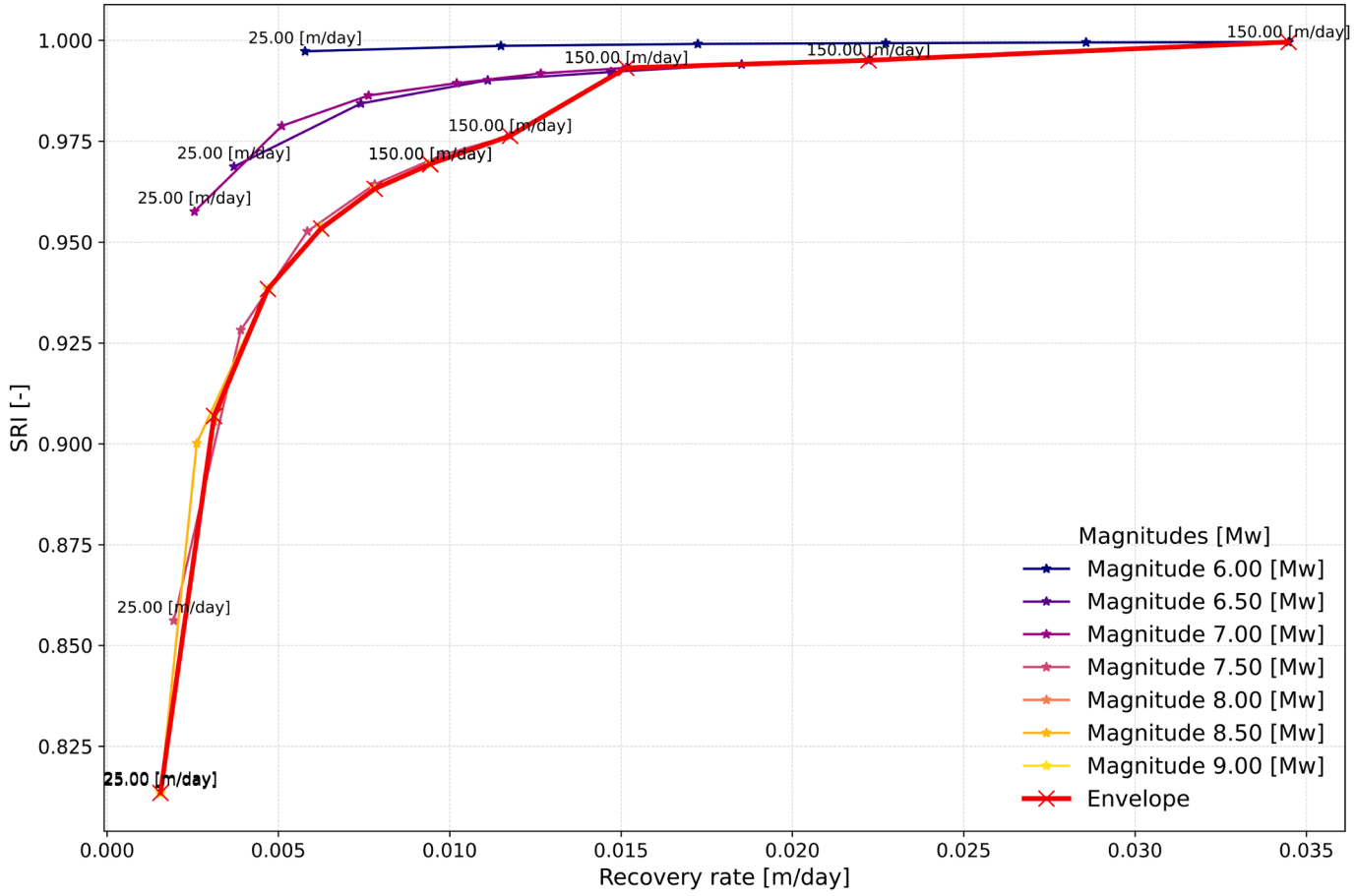

Fig. 9. Characteristic curves of SRI as a function of recovery rate for varying earthquake magnitudes in Network 1.

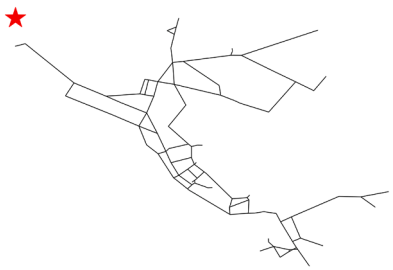

Fig. 10. Illustration of Network 3 from the EPANET example set and the location of the earthquake epicenter.

The near-optimal strategy exhibits an early and sustained increase in SDI, indicating efficient prioritization of critical pipelines that contribute meaningfully to network recovery.

The shape of the SDI curve for the GA solution is consistent with a convex profile, suggesting a deliberate focus on pipelines with the highest marginal impact on performance. In contrast, both baseline strategies exhibit delayed recovery. The head-based strategy (blue curve) initiates repairs on pipelines with limited influence on SDI, resulting in an extended initial plateau and a slower overall recovery trajectory. Similarly, the demand-based strategy (yellow curve) allocates early repair efforts to less critical components, yielding minimal performance gains until a significant portion of the network is restored.

The full recovery process in this scenario spans approximately 2500 days (roughly 6.5 years), a timeline that would be operationally unacceptable in real-world post-earthquake recovery. Notably, a prolonged plateau is observed between days 1200 and 1,800, corresponding to the repair of a single 14 km pipeline. At 25 m/day, this repair alone requires over 500 days to complete, underscoring the limitations of constrained resource environments.

The GA-optimized sequence is also compared against one obtained by a more computationally efficient method, the dynamic importance (DI) ranking heuristic of Section 3.1 (Fig. 13a and Table 3). DI ranking builds the repair sequence greedily: at each step it repairs the not-yet-repaired pipe whose restoration yields the largest immediate gain in SDI, re-ranking the remaining pipes after every repair, so it reaches a sequence in far fewer hydraulic evaluations than the GA's population search; the comparison is therefore primarily one of computational efficiency.[1] On Network 1, DI ranking attains an active-horizon SRI of 0.61, within the static-importance baseline spread (0.54–0.67) and trailing the GA (0.82), while needing only 80 hydraulic evaluations versus the GA's 37,200, meaning a roughly 465-fold reduction. On this small, tank-buffered network the heuristic is thus comparable to the static baselines but does not close the gap to the GA.

The advantage of the dynamic heuristic becomes decisive on the larger Network 3 (Fig. 13b and Table 3). Here the full GA optimization is computationally demanding; of the order of 10^6 pressure-dependent hydraulic simulations per scenario, requiring the high-performance computing resources discussed in Section 6, whereas DI ranking produces its sequence in about 5,000 evaluations on a standard laptop. More importantly, DI ranking reaches an active-horizon SRI of 0.63, roughly

[1] For a controlled comparison, the curves in Fig. 13 are computed for all strategies within one shared evaluator; the resulting absolute SRI values differ from those in Figs. 6 and 12, produced with the original pipeline. The GA's advantage over the heuristic and static strategies is preserved under this shared normalization.

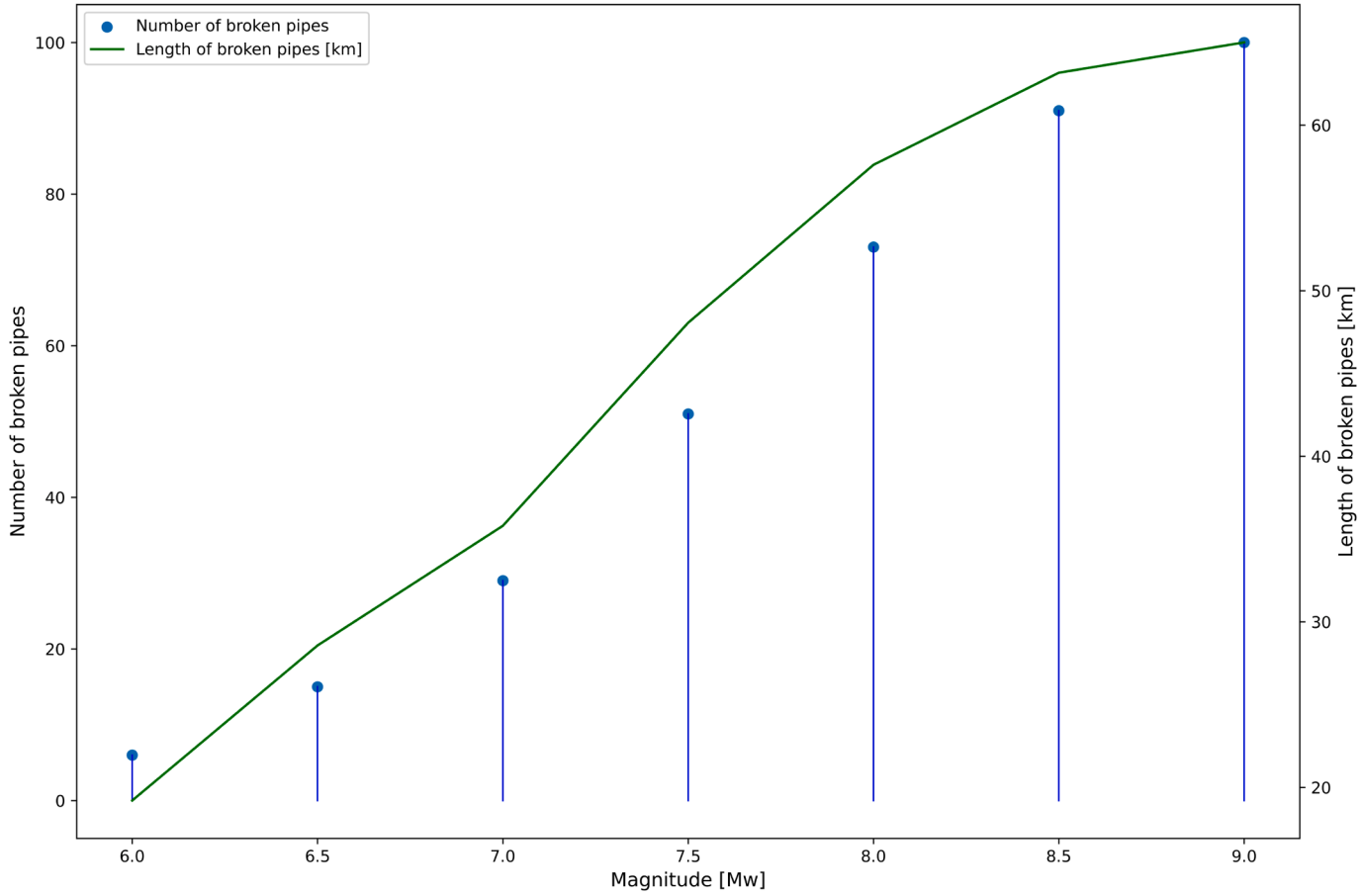

Fig. 11. Number and length of broken pipes versus earthquake magnitudes for Network 3.

Table 3
Repair-sequencing strategies under one shared evaluator (M_w 9.0, one crew at 25 m/day). Active-horizon SRI is the time-averaged SDI over the repair window.

Network	Strategy	Active-horizon SRI	Hydraulic solves	Wall-clock
Network 1 (12 pipes)	GA (optimal)	0.82	37,200	~26 min (laptop)
	DI ranking	0.61	80	3.4 s
	Demand ranking	0.67	12	< 1 s
	Head ranking	0.54	12	< 1 s
Network 3 (100 pipes)	GA (optimal)	(0.698)*	~10^6	days (HPC / DelftBlue)
	DI ranking	0.63	5,052	~52 min (laptop)
	Demand ranking	0.26	100	< 1 min
	Head ranking	0.36	100	< 1 min

*Value corresponding to Fig. 12 (DelftBlue); only shown for reference, not recomputed in this controlled local comparison.

doubling both static baselines (0.36 for head-based and 0.26 for demand-based ranking). The contrast with Network 1 is itself informative: the value of dynamically re-ranked importance over static ranking grows with network size and connectivity, precisely the regime in which exhaustive metaheuristic search becomes impractical.

To investigate the impact of increased repair capacity, two additional scenarios with the same earthquake magnitude (9.0 Mw) but higher repair rates are considered: 75 m/day (three repair crews) and 150 m/day (six repair crews). Fig. 14 illustrates the results for the 75 m/day case. Here, the near-optimal strategy achieves an SRI of 0.896, compared to 0.791 for the average head-based strategy and 0.757 for the demand-based strategy. The total recovery duration is reduced to approximately 1000 days (under three years), demonstrating the value of increased repair capacity.

Fig. 15 displays the results for the highest resource scenario, with a repair rate of 150 m/day (six crews). In this case, the GA solution yields an SRI of 0.948, whereas the head-based and demand-based strategies result in SRI values of 0.895 and 0.879, respectively. The network is fully restored within approximately 500 days, indicating an almost five-fold reduction in recovery time relative to the single-crew scenario.

These findings highlight that while increased repair rates substantially reduce recovery time, the gains in overall resilience-as measured by the SRI-are less than proportional. Specifically, increasing the repair rate from 25 m/day to 150 m/day results in a reduction in recovery time of approximately 80%, but only a 36% improvement in the SRI. This discrepancy suggests diminishing returns with respect to resilience when solely increasing resource allocation, indicating the need for strategic planning in resource deployment.

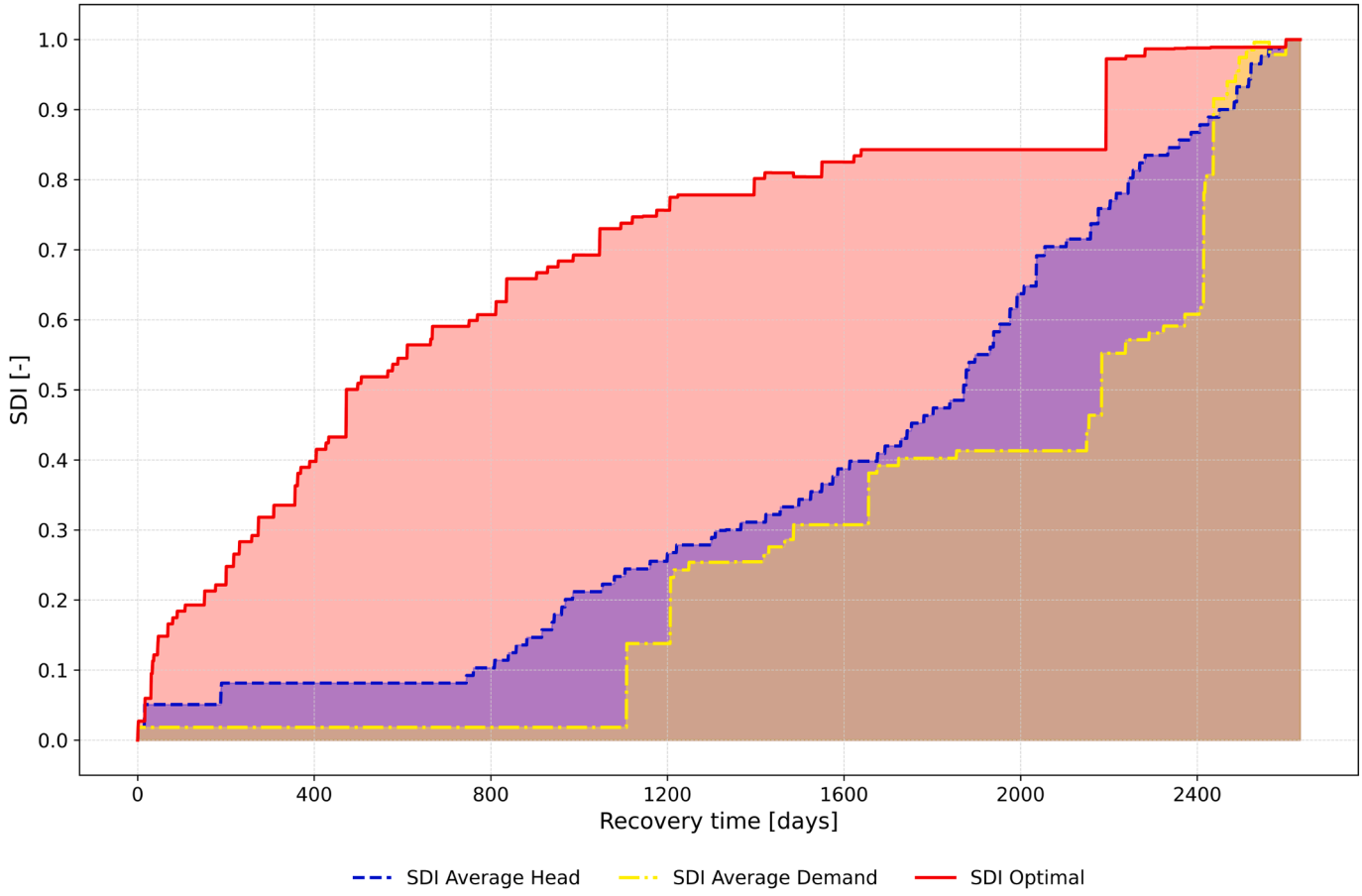

Fig. 12. Recovery curve of Network 3 with one crew (25 m/day repair rate).

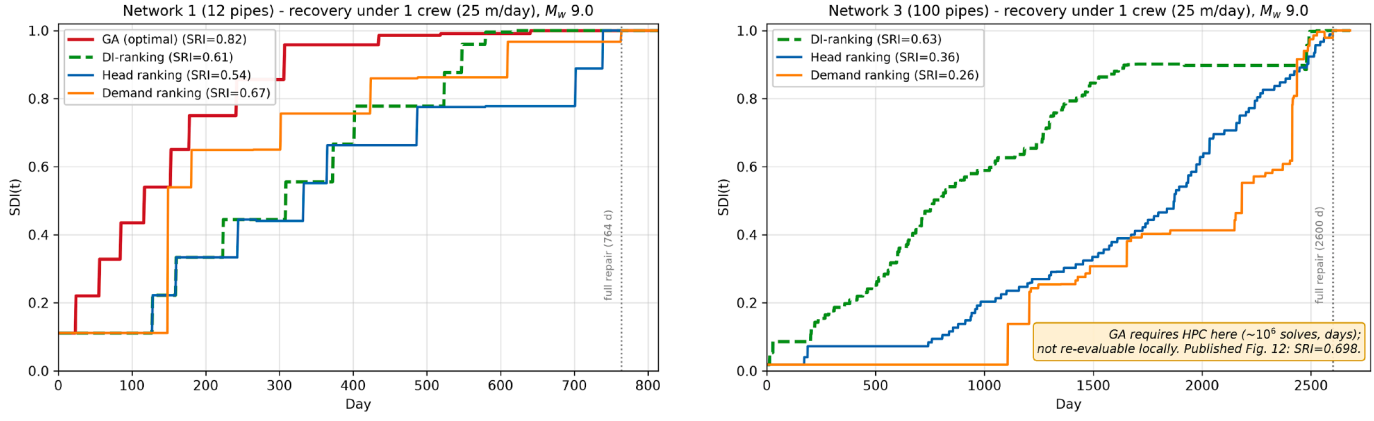

(a) Network 1 (12 damaged pipes)

(b) Network 3 (100 damaged pipes)

Fig. 13. Controlled comparison of repair-sequencing strategies under a single shared hydraulic/recovery/SDI evaluator (M_w 9.0, one crew at 25 m/day). On the small Network 1 (a) the GA leads and DI ranking is comparable to the static baselines; on the large Network 3 (b) the GA is computationally infeasible without high-performance computing, while DI ranking roughly doubles the resilience of both static baselines. The value of the dynamic heuristic over static ranking grows with network size.

For this larger network, the number of generations was increased to 100; all other GA settings are as in Case 1. The performance of the GA is further evaluated using a box plot of the fitness values across generations, as shown in Fig. 16. The persistence of outliers and variability in later generations suggest that the algorithm has not yet fully converged, likely due to the increased complexity and size of Network 3. Additional generations or alternative optimization strategies may be necessary to enhance convergence reliability for large-scale networks. The corresponding box-plots for the three- and six-crew cases (75 and 150 m/day) are reported in the Appendix (Figs. A.1 and A.2).

5.2.3. *Characteristic curves*

This section presents the characteristic curves for Network 3, following the same methodology as outlined in the first case study. While the

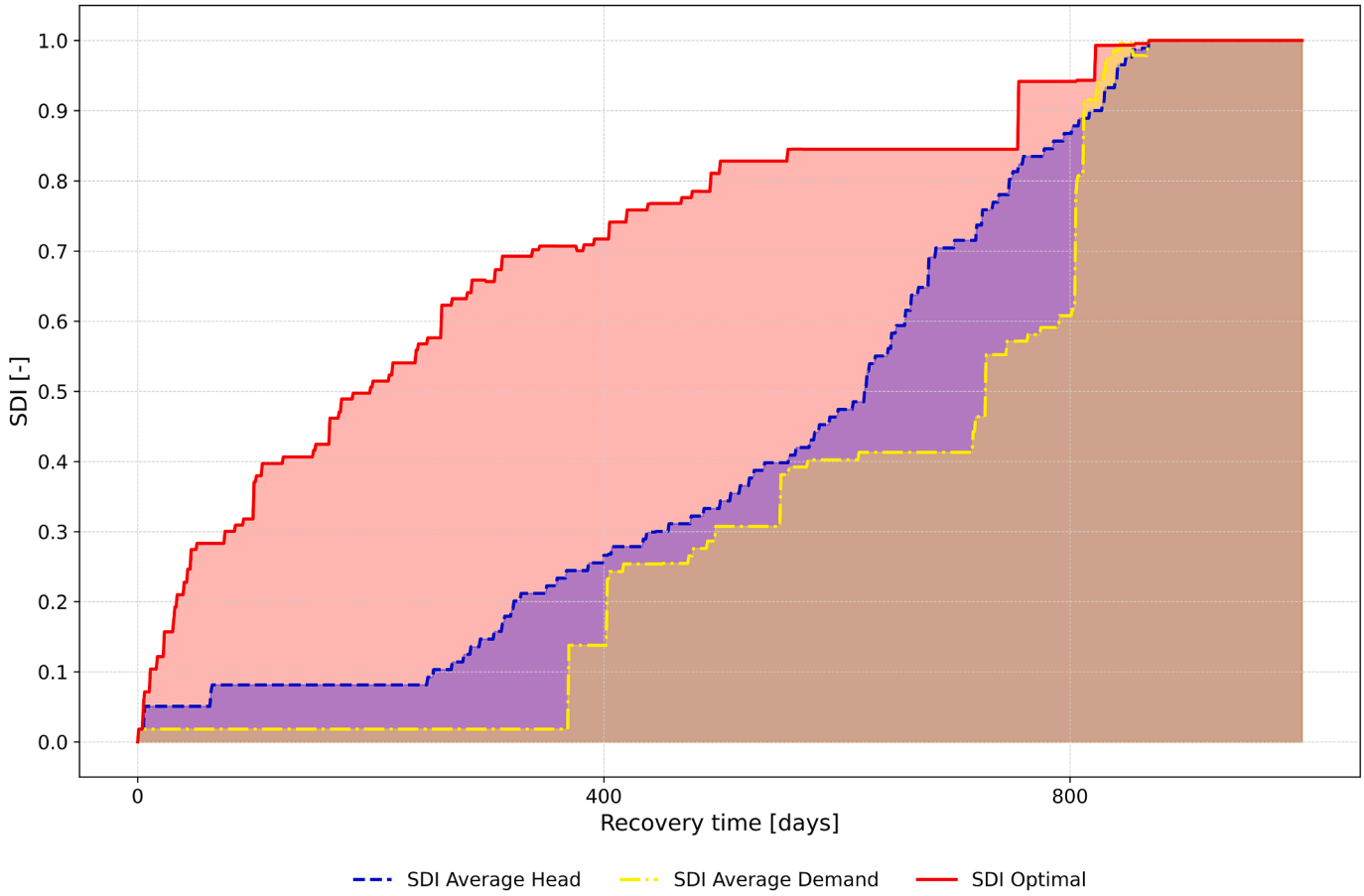

Fig. 14. Recovery curve of Network 3 with three crews (repair rate of 75 m/day).

general trends observed in Section 5.1 remain valid, the increased scale and complexity of Network 3 introduce additional challenges and lead to more nuanced behavior during the recovery process.

Fig. 17 illustrates the relationship between the SRI and the recovery rate for various levels of repair capacity. Each curve corresponds to a different number of repair crews, with repair rates ranging from 25 m/day (1 crew) to 150 m/day (6 crews). Points along each curve represent earthquake magnitudes ranging from 6.0 Mw to 9.0 Mw, increasing from top to bottom.

In contrast to Network 1, where a 6.0 Mw event did not significantly affect network performance, Network 3 exhibits a measurable decline in SRI even at the lowest magnitude. This suggests that the higher connectivity and inter-dependencies among components in larger systems can amplify the effects of minor disruptions. Moreover, even under the most favorable conditions-i.e., a maximum repair rate of 150 m/day-the network fails to achieve $SRI = 1.0$ at the highest magnitude, indicating that full recovery is unattainable with the available resources. Interestingly, the network also does not reach perfect resilience at 6.0 Mw, highlighting its increased vulnerability due to scale and system interdependence.

The expected trend of proportional increases in recovery rate with rising repair capacity remains evident, particularly for lower magnitudes. However, the absolute recovery rates achieved in Network 3 are consistently lower than those observed in Network 1. This observation underscores the greater resource demands and inherent structural complexity associated with larger networks.

Fig. 18 presents the SRI as a function of recovery rate for various earthquake magnitudes. Compared to the results for Network 1, several differences are immediately apparent. First, for smaller magnitudes such as 6.0 Mw, the SRI starts at a lower value even at minimal recovery rates, suggesting that Network 3 is more sensitive to moderate seismic activity. This sensitivity is likely due to the network's scale and the cumulative impact of minor component failures.

At higher magnitudes, such as 9.0 Mw, the initial SRI is significantly reduced, and recovery progresses more slowly. Even with increased repair capacity, the network struggles to approach full resilience, highlighting the difficulty of restoring service in large systems experiencing extensive damage.

An additional observation pertains to the convergence of the characteristic curves at higher repair rates. As more resources are deployed, the differences in SRI between varying magnitudes become less pronounced. This convergence suggests that increasing the recovery rate mitigates the effects of initial damage to some extent. Nevertheless, the lower nominal values of the recovery rate in Network 3 compared to Network 1 demonstrate the system's greater resistance to efficient restoration.

These results emphasize the importance of network-specific planning in seismic resilience assessment. While smaller networks may achieve near-complete recovery with moderate resource investment, larger and more interconnected systems demand significantly more resources and tailored strategies to ensure an effective recovery.

6. Discussion

This study proposed an optimization-based framework aimed at enhancing the post-seismic resilience of WDNs by identifying optimal repair sequences for damaged pipelines. The methodology integrates hydraulic simulation, seismic modeling, and an optimization model to

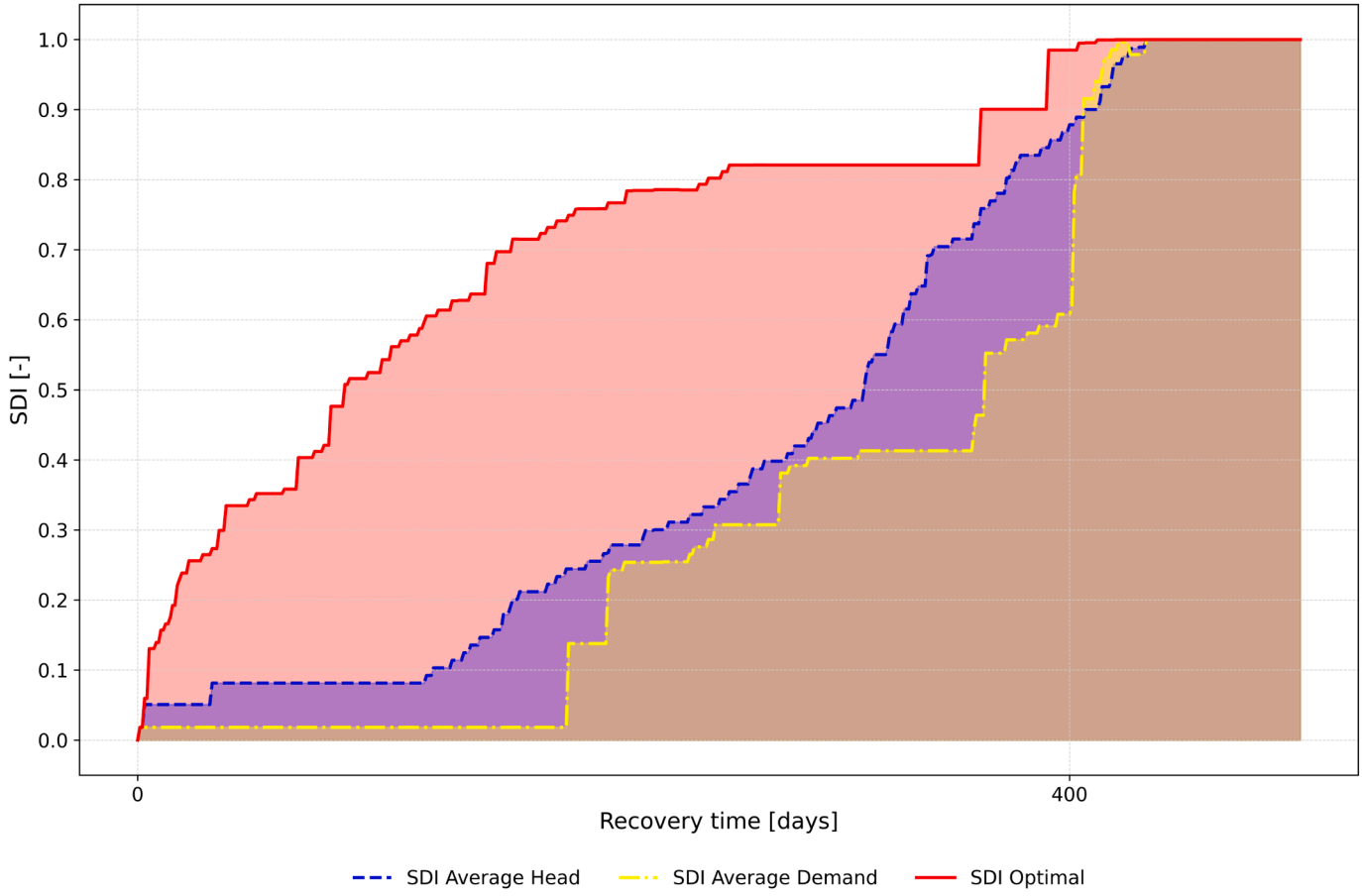

Fig. 15. Recovery curve of Network 3 with six crews (repair rate of 150 m/day).

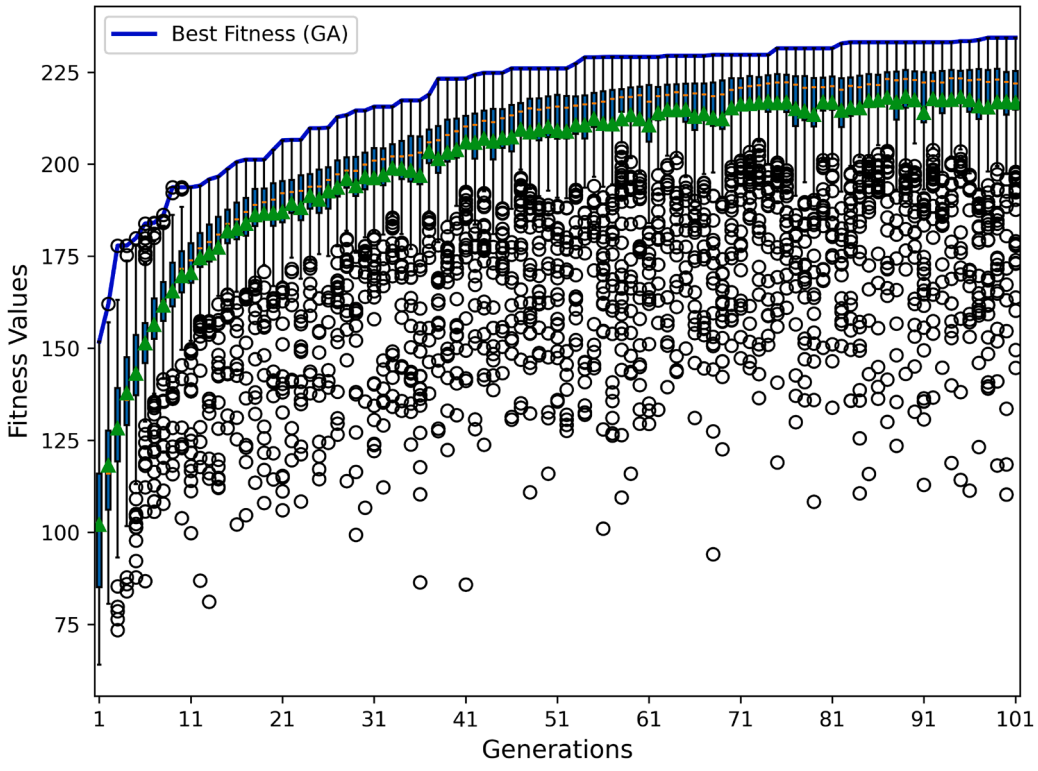

Fig. 16. Box plot of GA training for Network 3 with one crew (repair rate of 25 m/day). Symbols as in Fig. 7.

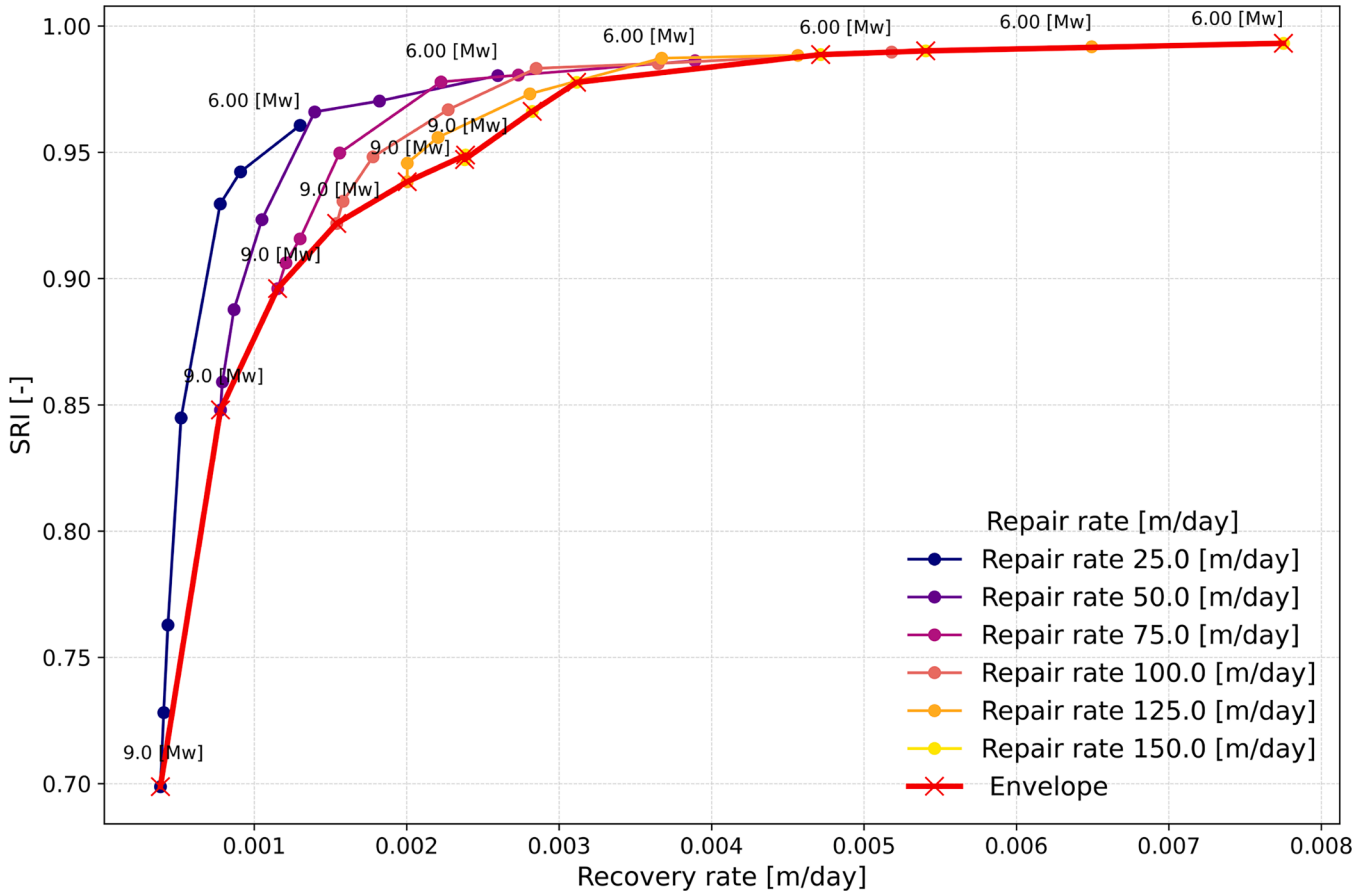

Fig. 17. Characteristic curves of SRI as a function of recovery rate for varying repair rates in Network 3.

derive effective recovery strategies. In addition, the study introduces the use of characteristic curves to evaluate the interplay between recovery resources, system damage levels, and overall network resilience.

The results highlight several key findings. First, the optimal repair sequence generated by the GA consistently achieves higher Seismic Resilience Index (SRI) values than fixed strategies based on average demand or average hydraulic head. The reason lies in the information available to each strategy: the GA evaluates every candidate sequence through the full hydraulic simulation of the recovery, so its ranking internalizes network topology, redundancy, and the evolving hydraulic state of the partially restored network. That is, it detects that restoring a particular trunk main reconnects entire demand clusters early, and defers repairs whose immediate hydraulic benefit is marginal. The fixed strategies, by contrast, rank the pipes once, using static and purely local attributes (the average nodal demand or head) that do not capture how the repair of one pipe conditions the benefit of the next; consequently, they may spend early repair capacity on pipes that remain hydraulically isolated until late in the recovery. By prioritizing critical pipes, the optimal approach promotes early-stage recovery and delivers greater overall performance across networks of differing size and complexity. In contrast, benchmark strategies exhibit greater variability and inefficiency, particularly in larger or more intricate networks.

The characteristic curves developed in this study provide valuable insights into the relationship between resource allocation, recovery rate, and resilience. They offer a visual representation of the achievable levels of recovery efficiency for different hazard levels and resource capacities. Moreover, the complexity of different networks is reflected in the shape and behavior of the characteristic curves, suggesting their potential use as a classification or benchmarking tool for infrastructure systems.

These findings broadly align with previous studies that emphasize the importance of recovery sequencing and optimization to improve post-disaster performance [25,26]. They also confirm the utility of GA-based methods for scheduling optimization under complex constraints [24]. However, the integration of characteristic curves into the recovery planning of WDNs constitutes a novel contribution. This addition enables a more comprehensive assessment by connecting resource planning with dynamic system behavior under stress.

One result that diverges from common assumptions is the observed non-linear benefit of increased repair capacity. While earlier research often implies proportional resilience gains from additional crews, the present study shows that, particularly in larger or more damaged networks, diminishing returns emerge. Beyond a certain threshold, more resources do not necessarily lead to proportional improvements in SRI, underscoring the value of strategic, rather than purely quantitative, allocation of resources.

Several limitations of the study must be acknowledged. The current model assumes that only one crew operates at a time, completing one pipeline repair before proceeding to the next. While this simplifies the simulation, it does not capture the benefits of simultaneous or parallel repair efforts. Incorporating multiple crew operations would likely improve realism but would also increase the model's complexity and computational demands. Additionally, the optimization process-particularly for larger networks-requires substantial computational resources. In the second case study, this necessitated the use of the Delft-Blue supercomputer at the Delft High Performance Computing Center (DHPC) [51]. The computational burden stems not from network size per se but from the analysis structure: each fitness evaluation requires a hydraulic simulation after every completed repair (up to 100 damaged pipes for Network 3 at 9.0 Mw), repeated for a population

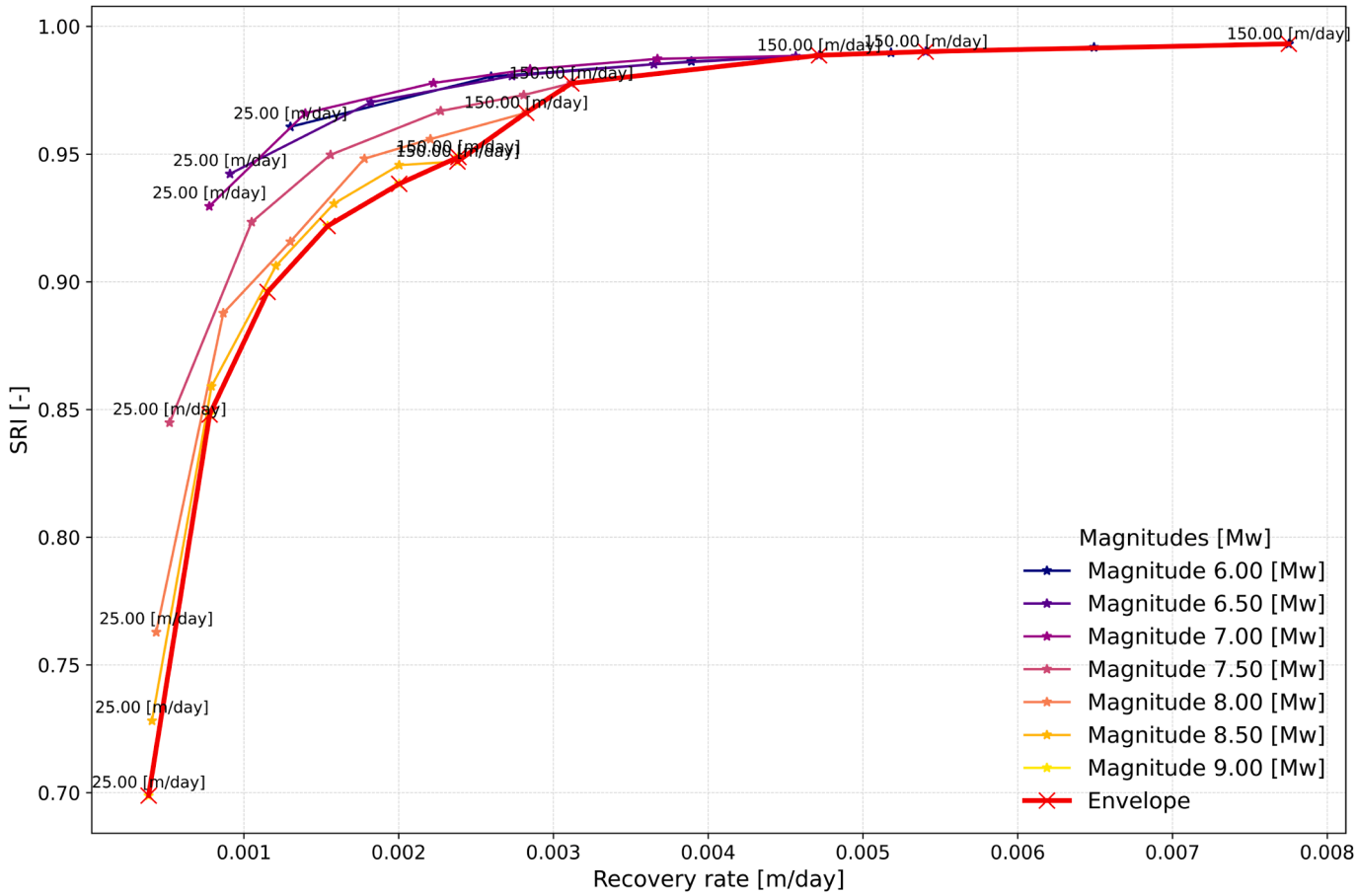

Fig. 18. Characteristic curves of SRI as a function of recovery rate for varying earthquake magnitudes in Network 3.

of 100 sequences across the search generations, with the entire optimization rerun for every combination of earthquake magnitude and repair capacity needed to build the characteristic curves, resulting in millions of hydraulic simulations in total. Part of this cost is an artifact of the present implementation rather than of the method itself: each post-repair state is solved independently rather than warm-started from the preceding step, and warm-starting across consecutive repairs is a straightforward, substantial speed-up that leaves the computed recovery sequences unchanged—left to future work. Costs of this order are not unusual for repair-sequence optimization on large systems [29], and dynamic importance-ranking heuristics and learning-based surrogates [20,26,30] are promising routes to reducing it. To confirm that the burden originates in the number of fitness evaluations rather than in the search itself, we implemented the dynamic importance-ranking heuristic under an identical hydraulic, damage, and crew model (Section 3.1); it produces sensible recovery sequences in 10^2–10^4 hydraulic evaluations, against the GA's $\sim 10^6$, which localizes the computational cost in the repeated pressure-dependent simulation, not in the optimization. This dependence on high-performance computing may limit practical adoption in settings with constrained computational infrastructure.

The modeling scope also entails simplifications that suggest avenues for refinement. The framework focuses on buried pipelines and does not model damage to reservoirs, tanks, pumping stations, or water treatment plants, which recent studies and post-event observations show can govern service loss in severe events [36,37]. The seismic input is likewise represented through magnitude- and distance-dependent intensities, without resolving site-to-site hazard variability across large networks or local site effects such as soil amplification and liquefaction-induced permanent ground deformation, which are known to amplify pipeline damage in soft or saturated soils [33,52,53]; incorporating spatially correlated ground motions and site-specific amplification would add realism for region-scale applications. The damage model also treats failed pipes as closed and repaired over their full length, implicitly assuming failures are promptly detected and isolated; representing leaks explicitly through pressure-dependent discharge and modeling point repairs of individual breaks, as in the Battle of Post-Disaster Response and Restoration [28,47], is a natural refinement, together with a graded damage description that separates intermediate damage levels from complete loss of the pipe (Section 2.4). Finally, evaluating ensembles of damage realizations per earthquake magnitude would endow the characteristic curves with confidence bands reflecting damage-sampling uncertainty.

Despite these limitations, the findings have important implications for practice. For asset managers and infrastructure operators, the model provides a structured tool for planning pipeline repair sequences and allocating resources effectively. The use of characteristic curves offers a practical means to evaluate whether the available resources are sufficient to meet resilience goals under different hazard scenarios. By simplifying complex system dynamics into interpretable insights, the framework can support data-informed decisions in emergency preparedness and recovery planning.

To strengthen the framework, future research should consider expanding the model to allow for parallel and dynamic crew operations. Incorporating variable node importance could better capture the needs of critical consumers such as hospitals, emergency services, or shelters, for instance through multi-indexed nodal-importance weighting schemes [38]. The resilience assessment could also benefit from embedding economic considerations, enabling cost-benefit analysis of resource deployment strategies. Furthermore, the framework could be adapted to assess other hazards, such as floods, wildfires, or cyber-attacks, thereby

increasing its applicability. Finally, tailoring characteristic curves with performance thresholds for specific systems and hazard types would enhance their decision-support utility and improve the capacity of the model to guide long-term resilience planning. Embedding life-cycle considerations could further enhance maintenance prioritization for important networks [54,55]. We have implemented the dynamic importance-ranking heuristic of [20,26] under an identical hydraulic, damage, and crew model and report the comparison in Section 5 (Fig. 13, Table 3): the heuristic recovers a competitive recovery sequence at a small fraction of the GA's cost and, on the larger network, clearly outperforms the static importance baselines. A corresponding comparison against reinforcement-learning solvers [30] remains future work, as it requires training a dedicated graph-neural-network surrogate on many simulated recovery episodes, which falls outside the present scope.

7. Conclusion

This study presented a framework to optimize the post-seismic recovery of water distribution networks by combining hydraulic simulation, seismic damage modeling, and an optimization engine to determine the most effective sequence for repairing damaged pipelines. The results demonstrate that prioritizing repairs strategically, rather than following fixed, demand-based or head-based orders, significantly reduces restoration time and improves overall service continuity. The GA-optimized sequences were further benchmarked against a low-cost dynamic importance-ranking heuristic, which recovers competitive sequences at a small fraction of the computational cost and whose advantage over the static demand- and head-based rankings grows with network size.

An important insight from the analysis lies in the non-linear benefits of adding repair crews. For moderate disruptions, increasing the daily repair rate leads to proportional improvements in the time needed to regain normal service. However, when facing higher damage levels, even large increases in resource allocation yield diminishing returns. These findings emphasize the need for a thoughtful balance between resource availability and other resilience measures, such as system redundancies or pipeline upgrades.

The paper also introduced characteristic curves as a means to visualize how different repair capacities affect network performance under a range of seismic intensities. These curves highlight thresholds beyond which additional repair crews do not translate into proportional improvements in resilience. Such observations suggest that network-specific factors-including pipe lengths, connectivity patterns, and hydraulic dependencies-govern recovery outcomes more strongly than raw repair capacity alone.

Although the proposed framework was tested on two networks of different sizes, the modeling approach and optimization process are broadly applicable. The results indicate that increasing the scale and interdependencies of a network amplifies the impact of moderate seismic events and prolongs the recovery process, reinforcing the value of early-stage planning. One limitation is that the current approach treats the available crews as a single team that repairs one pipe at a time. Future research can extend the method to account for multiple teams working in parallel, incorporate dynamic crew sharing among different locations, or integrate cost-related objectives to enable more comprehensive decision-making (Table A.1).

CRediT authorship contribution statement

V. Tsioni: Writing – original draft, Visualization, Validation, Methodology, Formal analysis, Conceptualization; **O. Kammouh:** Writing – review & editing, Writing – original draft, Visualization, Validation, Supervision, Software, Resources, Project administration, Methodology, Data curation, Conceptualization; **M. Nogal:** Writing – review & editing, Writing – original draft, Visualization, Validation, Supervision, Software, Resources, Methodology, Formal analysis, Conceptualization.

Relevance to Resilience

Water distribution networks are critical urban lifelines: their post-earthquake performance conditions firefighting, healthcare, sheltering, and the pace at which urban life resumes. This work contributes to urban resilience in three ways. First, it quantifies resilience explicitly through a Seismic Resilience Index measuring cumulative satisfaction of user demand over the recovery horizon. Second, it allows rapid resilience enhancement by identifying the repair sequence that restores service fastest for the available crew. Third, it supports preparedness and resource planning by introducing characteristic curves that map the resilience achievable for any combination of earthquake intensity and repair capacity. With these curves, utilities and planners can determine in advance the crew capacity required to meet recovery targets for a given hazard level, compare networks of different size and topology on a common basis, and identify thresholds beyond which added resources no longer yield proportional resilience gains. The framework thus links component-level seismic damage to city-level service recovery, supporting both pre-event preparedness and post-event response.

Declaration of generative AI and AI-assisted technologies in the writing process

During the preparation of this work, the authors used ChatGPT in order to improve the grammar and readability of the text. After using this tool, the authors reviewed and edited the content as needed, and take full responsibility for the content of the publication.

Declaration of competing interest

The authors declare that they have no known competing financial interests or personal relationships that could have appeared to influence the work reported in this paper.

Appendix A.

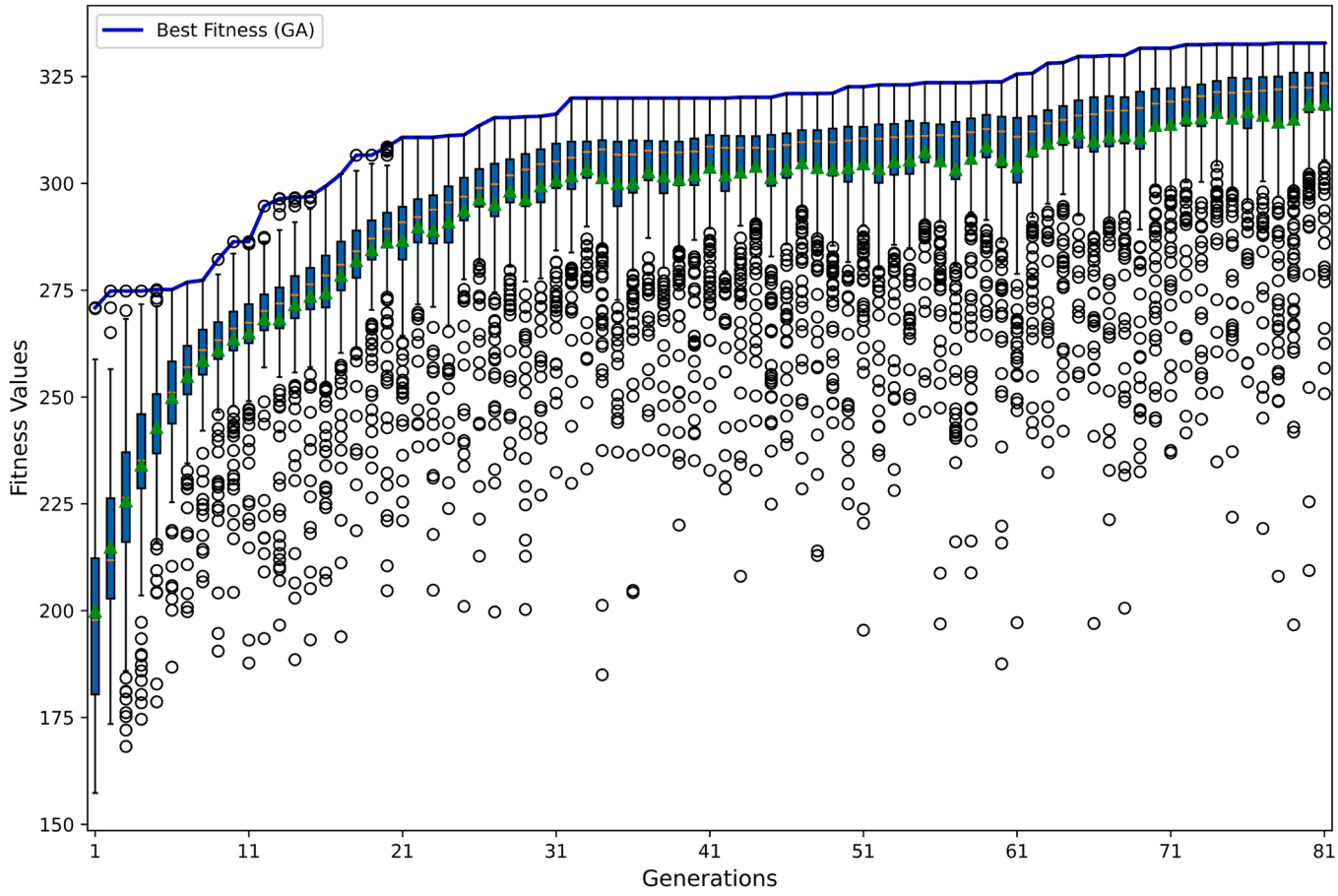

Fig. A.1. Box-plot of GA training for Network 3 with three crews (repair rate of 75 m/day).

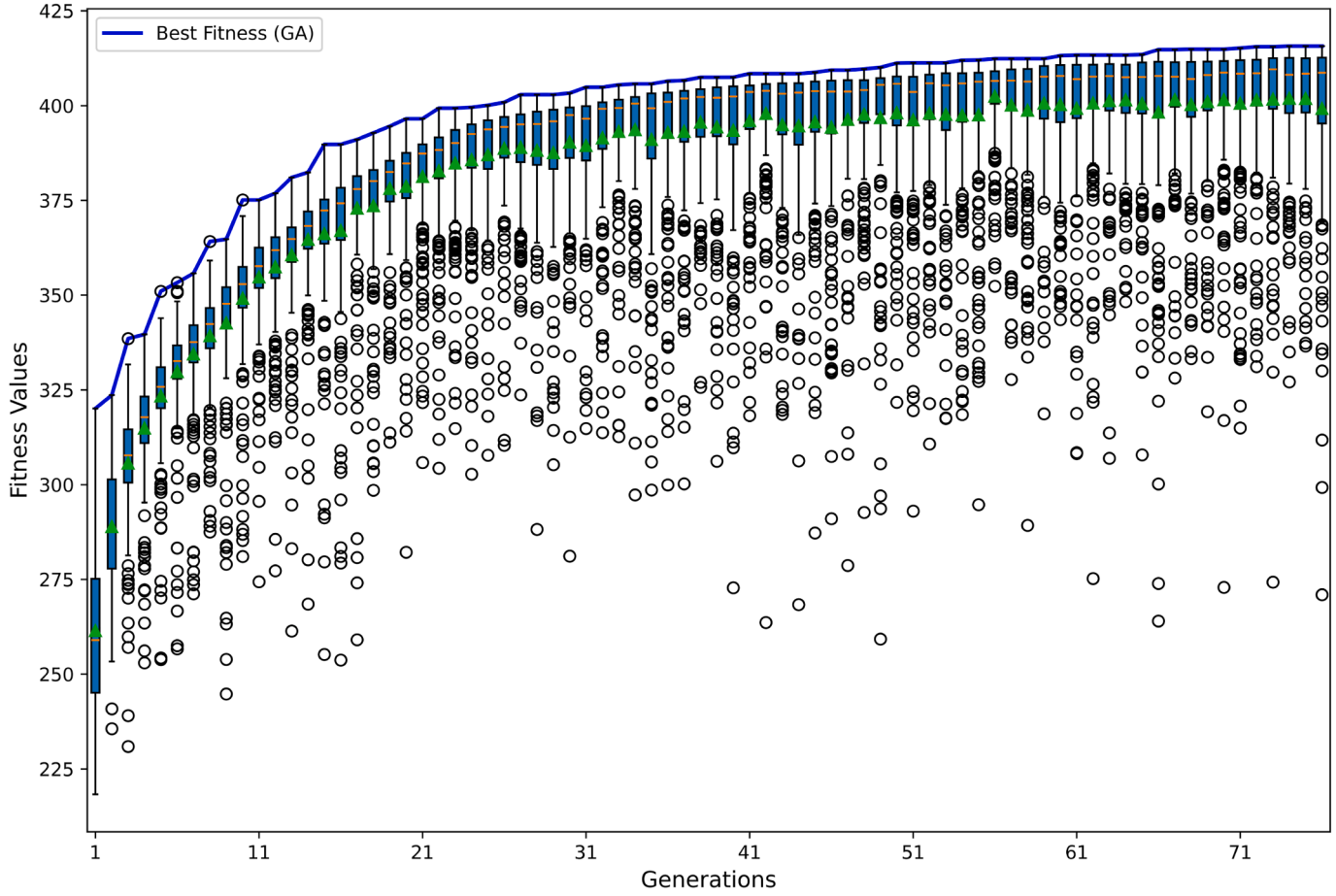

Fig. A.2. Box-plot of GA training for Network 3 with six crews (repair rate of 150 m/day).

Table A.1
Complete table with pipe name and lengths for Network 3.

Pipe IDs	Length (km)	Pipe IDs	Length (km)
20	0.03	195	0.01
40	0.03	199	0.06
50	0.03	201	0.36
60	0.37	202	0.03
101	4.32	203	0.15
103	0.41	204	1.39
105	0.77	205	0.40
107	0.45	207	0.41
109	1.20	209	0.15
111	0.61	211	0.20
112	0.35	213	0.78
113	0.51	215	0.37
114	0.61	217	0.16
115	0.60	219	0.11
116	0.50	221	0.70
117	0.83	223	0.35
119	0.66	225	0.85
120	0.22	229	1.22
121	0.57	231	0.19
122	0.62	233	0.03
123	0.61	235	0.22
125	0.46	237	0.36
129	0.28	238	0.13
131	0.98	239	0.43
133	0.24	240	0.15
135	0.27	241	0.27
137	1.98	243	0.37
145	0.84	245	0.30
147	0.62	247	1.30
149	0.42	249	0.50
151	0.50	251	0.62
153	1.07	257	0.48
155	0.67	261	0.67
159	0.27	263	0.59
161	0.31	269	0.63
163	0.36	271	0.24
169	1.39	273	0.15
171	1.05	275	0.01
173	0.63	277	0.67
175	0.89	281	0.13
177	0.61	283	0.13
179	0.13	285	0.01
180	0.05	287	0.42
181	0.15	289	0.28
183	0.18	291	0.33
185	0.02	293	0.33
186	0.03	295	0.44
187	0.39	297	0.19
189	0.01	193	0.01
191	0.23	–	–

References

[1] National Infrastructure Advisory Council (NIAC). Critical infrastructure resilience: Final report and recommendations. Technical Report; U.S. Department of Homeland Security; Washington, D.C.; 2009. Visited on 2023-11-14; https://www.cisa.gov/resources-tools/resources/niac-critical-infrastructure-resilience-final-report-and-recommendations.

[2] Assad A, Moselhi O, Zayed T, et al. A new metric for assessing resilience of water distribution networks. Water 2019;11(8):1701. Number: 8 Publisher: Multidisciplinary Digital Publishing Institute; https://doi.org/10.3390/w11081701

[3] Kammouh O, Fecarotti C, Marandi A, et al. A scalable optimization approach to the intervention planning of complex interconnected infrastructures. Reliab Eng Syst Saf 2024;250:110281. https://doi.org/10.1016/j.ress.2024.110281

[4] Arango E, Nogal M, Yang M, Sousa HS, Stewart MG, Matos JC, et al. Dynamic thresholds for the resilience assessment of road traffic networks to wildfires. Reliab Eng Syst Saf 2023;238:109407. https://doi.org/10.1016/j.ress.2023.109407

[5] Fragiadakis M, Christodoulou S, Vamvatsikos D, et al. Reliability assessment of urban water distribution networks under seismic loads. Water Resour Manag 2013;27. https://doi.org/10.1007/s11269-013-0378-0

[6] Bruneau M, Chang SE, Eguchi RT, Lee GC, O'Rourke TD, Reinhorn AM, et al. A framework to quantitatively assess and enhance the seismic resilience of communities. Earthq Spectra 2003;19(4):733–52. https://doi.org/10.1193/1.1623497

[7] De Iuliis M, Kammouh O, Cimellaro GP, Tesfamariam S. Quantifying restoration time of pipelines after earthquakes: comparison of bayesian belief networks and fuzzy models. Int J Disaster Risk Reduct 2021;64:102491. https://doi.org/10.1016/j.ijdrr.2021.102491

[8] Kammouh O, Cimellaro GP, Mahin SA. Downtime estimation and analysis of lifelines after an earthquake. Eng Struct 2018;173:393–403. https://doi.org/10.1016/j.engstruct.2018.06.093

[9] Todini E. Looped water distribution networks design using a resilience index based heuristic approach. Urban Water 2000;2(2):115–22. https://doi.org/10.1016/S1462-0758(00)00049-2

[10] Creaco E, Franchini M, Todini E, et al. The combined use of resilience and loop diameter uniformity as a good indirect measure of network reliability. Urban Water J 2016;13(2):167–81. Publisher: IAHR Website_eprint: https://doi.org/10.1080/1573062X.2014.949799

[11] Prasad TD, Hong S-H, Park N, et al. Reliability based design of water distribution networks using multi-objective genetic algorithms. KSCE J Civ Eng 2003;7(3):351–61. https://doi.org/10.1007/BF02831784

[12] Creaco E, Franchini M, Todini E. Generalized resilience and failure indices for use with pressure-driven modeling and leakage. J Water Resour Plan Manag 2016;142(8):04016019. https://doi.org/10.1061/(ASCE)WR.1943-5452.0000656

[13] Greco R, Di Nardo A, Santonastaso G, et al. Resilience and entropy as indices of robustness of water distribution networks. J Hydroinformatics 2012;14(3):761–71. https://doi.org/10.2166/hydro.2012.037

[14] Singh P, Gani A. Fuzzy concept lattice reduction using shannon entropy and huffman coding. J Appl Non-Class Log 2015;25. https://doi.org/10.1080/11663081.2015.1039857

[15] Yazdani A, Otoo RA, Jeffrey P. Resilience enhancing expansion strategies for water distribution systems: a network theory approach. Environ Model Softw 2011;26(12):1574–82. https://doi.org/10.1016/j.envsoft.2011.07.016

[16] Meng F, Fu G, Farmani R, Sweetapple C, Butler D. Topological attributes of network resilience: a study in water distribution systems. Water Res 2018;143:376–86. https://doi.org/10.1016/j.watres.2018.06.048

[17] Herrera M, Abraham E, Stoianov I, et al. A graph-theoretic framework for assessing the resilience of sectorised water distribution networks. Water Resour Manage 2016;30(5):1685–99. https://doi.org/10.1007/s11269-016-1245-6

[18] Marasco S, Cardoni A, Zamani Noori A, Kammouh O, Domaneschi M, Cimellaro GP. Integrated platform to assess seismic resilience at the community level. Sustain Cities Soc 2021;64:102506. https://doi.org/10.1016/j.scs.2020.102506

[19] Tabucchi T, Davidson R, Brink S. Simulation of post-earthquake water supply system restoration. Civ Eng Environ Syst 2010;Publisher: Taylor & Francis; https://doi.org/10.1080/10286600902862615

[20] Han Z, Ma D, Hou B, Wang W, et al. Seismic resilience enhancement of urban water distribution system using restoration priority of pipeline damages. Sustainability 2020;12(3):914. Number: 3 Publisher: Multidisciplinary Digital Publishing Institute; https://doi.org/10.3390/su12030914

[21] Zhao X, Chen Z, Gong H, et al. Effects comparison of different resilience enhancing strategies for municipal water distribution network: a multidimensional approach. Math Probl Eng 2015;2015(1):438063. https://doi.org/10.1155/2015/438063

[22] Chang SE, Shinozuka M. Measuring improvements in the disaster resilience of communities. Earthq Spectra 2004;20(3):739–55. Publisher: SAGE Publications Ltd STM; https://doi.org/10.1193/1.1775796

[23] Cimellaro GP, Tinebra A, Renschler C, Fragiadakis M, et al. New resilience index for urban water distribution networks. J Struct Eng 2016;142(8):C4015014. Publisher: American Society of Civil Engineers; https://doi.org/10.1061/(ASCE)ST.1943-541X.0001433

[24] Nozhati S. A resilience-based framework for decision making based on simulation-optimization approach. Struct Saf 2021;89. https://doi.org/10.1016/j.strusafe.2020.102032

[25] Farahmandfar Z, Piratla KR. Comparative evaluation of topological and flow-based seismic resilience metrics for rehabilitation of water pipeline systems. J Pipeline Syst Eng Pract 2018;9(1). https://doi.org/10.1061/(ASCE)PS.1949-1204.0000293

[26] Liu W, Song Z, Ouyang M, Li J, et al. Recovery-based seismic resilience enhancement strategies of water distribution networks. Reliab Eng Syst Saf 2020;203:107088. https://doi.org/10.1016/j.ress.2020.107088

[27] Song Z, Liu W, Shu S, et al. Resilience-based post-earthquake recovery optimization of water distribution networks. Int J Disaster Risk Reduct 2022;74:102934. https://doi.org/10.1016/j.ijdrr.2022.102934

[28] Paez D, Filion Y, Castro-Gama M, Quintiliani C, Santopietro S, Sweetapple C, et al. Battle of postdisaster response and restoration. J Water Resour Plan Manag 2020;146(8):04020067. https://doi.org/10.1061/(ASCE)WR.1943-5452.0001239

[29] Zhang Q, Zheng F, Chen Q, Kapelan Z, Diao K, Zhang K, et al. Improving the resilience of postdisaster water distribution systems using dynamic optimization framework. J Water Resour Plan Manag 2020;146(2):04019075. https://doi.org/10.1061/(ASCE)WR.1943-5452.0001164

[30] Fan X, Zhang X, Yu XB. A graph convolution network–deep reinforcement learning model for resilient water distribution network repair decisions. Comput-Aided Civ Infrastruct Eng 2022;37(12):1547–65. https://doi.org/10.1111/mice.12813

[31] Huang H, Burton HV. Dynamic seismic damage assessment of distributed infrastructure systems using graph neural networks and semi-supervised machine learning. Adv Eng Softw 2022;168:103113. https://doi.org/10.1016/j.advengsoft.2022.103113

[32] Yang S, Zhang Y, Lu X, Guo W, Miao H. Multi-agent deep reinforcement learning based decision support model for resilient community post-hazard recovery. Reliab Eng Syst Saf 2024;242:109754. https://doi.org/10.1016/j.ress.2023.109754

[33] Zhang Y, Zhong Z, Hou B, El Naggar MH, Xu C, Du X. Framework for evaluation of seismic damage of water distribution networks. Earthq Eng Struct Dyn 2025;55(1):250–66. https://doi.org/10.1002/eqe.70077
[34] Alam MS, Simpson BG, Barbosa AR, Jung J, Parulekar N. Probabilistic seismic damage and loss assessment methodology for wastewater network incorporating modeling uncertainty and damage correlations. Earthq Spectra 2023;39(3):1435–72. https://doi.org/10.1177/87552930231180642
[35] Hou B, Xu Q, Zhong Z, Han J, Miao H, Du X. Seismic reliability evaluation of spatially correlated pipeline networks by quasi-Monte Carlo simulation. Struct Infrastruct Eng 2022;20(4):498–513. https://doi.org/10.1080/15732479.2022.2111445
[36] Hou B, Jia R, Ma T, Yuan M, Xu C. Seismic resilience assessment framework of urban water supply systems considering pipeline and water treatment plant damages. Reliab Eng Syst Saf 2026;268:112024. https://doi.org/10.1016/j.ress.2025.112024
[37] Toprak S, Wham BP, Nacaroglu E, Ceylan M, Dal O, Senturk AE. Impact of seismic geohazards on water supply systems and pipeline performance: insights from the 2023 Kahramanmaraş earthquakes. Eng Geol 2024;340:107681. https://doi.org/10.1016/j.enggeo.2024.107681
[38] Hou B, Ma X, Diao K, Zhong Z, Wu S. Seismic performance assessment of water distribution systems based on multi-indexed nodal importance. Water 2021;13(17):2362. https://doi.org/10.3390/w13172362
[39] Klise KA, Hart DB, Bynum M, Hogge J, Haxton T, Murray R, et al. Water Network Tool for Resilience (WNTR) user Manual: Version 0.2.3. Technical Report EPA/600/R-20/185; U.S. EPA Office of Research and Development; Washington, DC; 2020.
[40] Rossman LA. EPANET 2 users manual. 2000. https://nepis.epa.gov/Exe/tiff2png.cgi/P1007WWU.PNG?-r+75+-g+7+D%3A%5CZYFILES%5CINDEX%20DATA%5C00THRU05%5CTIFF%5C00001541%5CP1007WWU.TIF.
[41] Wagner JM, Shamir U, Marks DH, et al. Water distribution reliability: simulation methods. J Water Resour Plan Manag 1988;114(3):276–94. Publisher: American Society of Civil Engineers; https://ascelibrary.org/doi/10.1061/%28ASCE%290733-9496%281988%29114%3A3%28276%29. https://doi.org/10.1061/(ASCE)0733-9496(1988)114:3(276)
[42] Fragiadakis M, Christodoulou SE. Seismic reliability assessment of urban water networks. Earthq Eng Struct Dyn 2014;43(3):357–74. https://doi.org/10.1002/eqe.2348
[43] American Lifelines Alliance. Seismic fragility formulations for water systems. Technical Report; American Lifelines Alliance, ASCE and FEMA; Reston, VA; 2001.
[44] Bellagamba X, Bradley BA, Wotherspoon LM, Hughes MW. Development and validation of fragility functions for buried pipelines based on canterbury earthquake sequence data. Earthq Spectra 2019;35(3):1061–86. https://doi.org/10.1193/120917EQS253M
[45] Gehl P, Matsushima S, Masuda S. Investigation of damage to the water network of Uki city from the 2016 Kumamoto earthquake: derivation of damage functions and construction of infrastructure loss scenarios. Bull Earthq Eng 2021;19:685–711. https://doi.org/10.1007/s10518-020-01001-z
[46] Iannacone L, Gardoni P. Physics-based repair rate curves for segmented pipelines subject to seismic excitations. Sustain Resilient Infrastruct 2022;8(1):121–41. https://doi.org/10.1080/23789689.2021.2000146
[47] Bata MH, Carriveau R, Ting D SK. Urban water supply systems' resilience under earthquake scenario. Sci Rep 2022;12:20555. https://doi.org/10.1038/s41598-022-23126-8
[48] Gad AF. PyGAD: an intuitive genetic algorithm Python library. Multimed Tools Appl 2024;83:58029–42. https://doi.org/10.1007/s11042-023-17167-y
[49] Arango E, Nogal M, Sousa HS, Matos JC, Stewart MG. Resilience assessment in post-wildfire recovery of road transport networks by dynamic thresholds and characteristic curves. Reliab Eng Syst Saf 2025;264:111365.
[50] Rossman L, Clark R, Grayman W. Modeling chlorine residuals in drinking-water distribution systems. J Environ Eng 1994;120:803–20. https://doi.org/10.1061/(ASCE)0733-9372(1994)120:4(803)
[51] Delft High Performance Computing Centre (DHPC). DelftBlue Supercomputer (Phase 2). 2024. https://www.tudelft.nl/dhpc/ark:/44463/DelftBluePhase2.
[52] Castiglia M, Fierro T, Santucci de Magistris F. Pipeline performances under earthquake-induced soil liquefaction: state of the art on real observations, model tests, and numerical simulations. Shock Vib 2020;2020:8874200. https://doi.org/10.1155/2020/8874200
[53] Sarvanis GC, Karamanos SA, Vazouras P, Mecozzi E, Lucci A, Dakoulas P. Permanent earthquake-induced actions in buried pipelines: numerical modeling and experimental verification. Earthq Eng Struct Dyn 2018;47(4):966–87. https://doi.org/10.1002/eqe.3001
[54] Jayaram N, Srinivasan K. Performance-based optimal design and rehabilitation of water distribution networks using life cycle costing. Water Resour Res 2008;44(1):W01417. https://doi.org/10.1029/2006WR005316
[55] Chu J, Zhou Z, Ding X, Tian Z. A life cycle oriented multi-objective optimal maintenance of water distribution: model and application. Water Resour Manag 2022;36(11):4161–82. https://doi.org/10.1007/s11269-022-03246-6